Utilization of Soft Matter as a Structure Directing Agent for the Synthesis of Nanostructured Materials

by

Andrew Kacheff

A thesis

presented to the University of Waterloo

in fulfillment of the

thesis requirement for the degree of

Master of Science

in

Chemistry - Nanotechnology

Waterloo, Ontario, Canada, 2014

Declaration

I hereby declare that I am the sole author of this thesis. This is a true copy of the thesis, including any required final revisions, as accepted by my examiners.

I understand that my thesis may be made electronically available to the public.

Abstract

Sol-gel methods combined with the adaptive structuring properties of soft matter, have been used to create templates and synthesize mesoporous materials or nanoparticles from them. For example, micelles formed with non-ionic surfactants containing ethylene oxide have been previously used as templates to produce mesoporous silica with a particular structure. These templates are known to be dynamic and adaptable to temperature changes. When combining these surfactant micelle templates with a precursor, a silicate/surfactant hybrid micelle is formed, which was demonstrated to be dynamic as well. In a first step, this thesis explores further the structure and dynamics of these hybrid micelles, and up to which point they resemble the initial micelle. Tetraethylorthosilicate (TEOS) was used as the silica precursor to make silicate hybrid micelles using these non-ionic surfactants and their behaviour as a function of temperature and silicate concentration was investigated.

In a second step, we expand the concept of soft matter-based structuring directing objects by replacing micelles with O/W nanoemulsions prepared by Phase Inversion Composition. These structures were already used as nanoreactors and porosity templates, but their use was somehow limited by their liquid nature. Therefore, we explored if solid templates could be obtained by replacing the original paraffin oil by a mixture of oil and wax. We extended further the concept of using W/O nanoemulsions as nanoreactors by testing the preparation and use of W/O nanoemulsions, and preliminary results in this strudy show that Prussian Blue analogues could be successfully synthesized.

In a final step, we increased the system complexity further by combining structure-directing soft matter with inorganic nucleation and condensation in a one step

reaction where 3D porous micrometric silica particles are obtained in a one-pot fast synthesis, and resulting materials were tested for HPLC application.

Acknowledgements

I would like to thank my supervisor Professor Eric Prouzet for all of the support and guidance he provided. I learned not only a lot about science and soft chemistry, but also about the conduct and attitude required in doing research. I would also like to thank my committee members Professor Linda Nazar and Professor Jean Duhamel for their time and support. A special thank you goes to Lu Li from Professor Duahmel's lab for her help with the fluorescence studies and to my laboratory members, Moacir Forim from Tadeusz Gorecki's lab for help conducting the HPLC tests, and my family for their assistance and their continued support and encouragement throughout all of my work.

Table of Contents

List of Figures

List of Tables

List of Abbreviations

Brij35: $(C_2H_4O)_{\sim 23}C_{12}H_{26}O$

Brij98: C_{18}-$H_{35}(OCH_2CH_2)_{20}$-OH

DLS: Dynamic Light Scattering

EIP: Emulsion Inversion Point

HLB: Hydrophilic-Lipophilic Balance

MSDS: Material Safety Data Sheet

P123: EO_{20}-PO_{70}-EO_{20}

PEO: polyethylene oxide -$(CH_2CH_2O)_n$-

PIC: Phase Inversion Composition

PIT: Phase Inversion Temperature

SAXS: Small Angle X-ray Scattering

SEM: Scanning Electron Microscopy

Span80: sorbitane monooleate

TEOS: Tetraethyl orthosilicate

TNP10: Tergitol NP-10

Tween20: Polyoxyethylene sorbitan monolaurate

Tween80: ethoxy sorbitane monooleate ester

T15-S-12: Tergitol 15-S-12

T15-S-30: Tergitol 15-S-30

Chapter 1: Introduction

1.1 Background

This project is relevant to integrative syntheses as defined initially by S. Mann[1] and C. Sanchez,[2] and more recently by R. Backov.[3] Integrative chemistry spans the combination of soft chemistry methods with the use of soft matter systems used as either templates or nanomolds.[4] This emerging area in material chemistry, obviously resulting from previous works and studies carried out within the last 20 years, still provides a new vision to material chemistry, as it focuses first on the structure and function required for a given material to fulfill a given function, and combines/integrates methods and precursors to achieve this structure. My project will explore how some dynamic and adaptive structures relevant to soft matter, such as silicate hybrid micelles and nanoemulsions,[5-9] can be combined with methods that lead to the successful synthesis of mesoporous materials.[10] This domain was first explored by Hessien who reported how nanoemulsions can be tuned and combined with usual silica sol-gel methods.[10] My project focuses more on explaining the dynamic behavior of templates (like silicate hybrid micelles) by extending the knowledge on existing materials and using them to make mesoporous materials. Therefore, I will combine methods and know-how relevant to sol-gel, soft chemistry, soft matter, and templating processes. A summary of the prior art in these domains is provided hereafter.

1.2 Soft Chemistry

Soft chemistry and soft matter stems from the idea of "chimie douce" developed by French scientists Jacques Livage and Jean Rouxel. The main goal was to develop

more advanced and complex materials because those prepared by high temperature methods target only thermodynamically stable phases. Indeed, materials synthesized at high temperature can hardly provide many of the properties and functions that can be achieved through soft chemistry such as permeability, porosity, high surface area, and multi-functionality. Soft chemistry, which is related to room temperature methods combining organic and inorganic moieties in order to achieve metastable states, is directly linked to sol-gel chemistry and the hybrid materials that come from it, synthesis of mesoporous and hierarchically structured materials, and designing thin and ultra-thin films from porous materials.[2] Classical preparation of inorganic materials is typically conducted at relatively high temperatures (quite often the melting temperatures of the materials being used). Soft chemistry uses low temperature to synthesize inorganic materials. The synthesis of materials at low temperature also increases the purity of the materials and arguably allows for much easier tunability.[11]

1.3 Sol-Gel Methods

Sol-gel chemistry spans most of the methods that involve the creation of inorganic or hybrid solid frameworks at room or moderate temperature. Ebelman and Graham were two of the investigators who observed that the hydrolysis of tetraethyl orthosilicate (TEOS) formed glass-like silicon dioxide.[12] For example, a network can be created by the polymerization of metal alkoxide precursors denoted by $M\text{-}(OR)_n$ where M is the metal center and RO groups are alkoxides that can have varying alkyl chains to form glass-ceramics.[13-14] In the activation step of the metal alkoxide, it undergoes a reaction of hydrolysis that creates terminal OH groups in place of the alkoxide OR groups (1). Then

the 3D polymerization occurs through a condensation that links metal centers via a M-OH-M bond, named olation (2) or a M-O-M bond named oxolation (3).[15-16] The letter X denotes either a hydrogen or another alkyl chain.

$$\text{M-OR} + \text{H-O-H} \longrightarrow \text{M-OH} + \text{R-OH} \quad (1)$$

$$\text{M-OH} + \text{X-OM} \longrightarrow \text{M-(OH)-M-OX} \quad (2)$$

$$\text{M-OH} + \text{X-OM} \longrightarrow \text{M-O-M} + \text{X-OH} \quad (3)$$

With this type of sol-gel methods, the solvent is usually the alcohol parent of the $M(OR)_n$ alkoxide and water is used as a reagent. The structure formed through condensation is greatly affected by the synthesis conditions. Depending upon the concentration of metal oxide precursors, amount of water, pH of the solution, temperature of solution, and the rate of condensation, the structure of the gelled network will vary.[17-20] Most of the metal alkoxides are very reactive in the presence of water or even water traces, whereas silicon alkoxides are generally quite inert and react only when hydrolysis and condensation catalysts (acid, base, fluoride) are added. Depending on the reaction kinetics and the way that the sol-gel is processed after reaction, one can generalize the final product as a gel or a powder. Generally speaking, gels will be formed when the nucleation and growth mechanism is hindered and powders will form when the nucleation and growth mechanism is accelerated.[21]

1.4 Soft Matter Systems

1.4.1 Emulsions

Emulsions consist of two immiscible liquid phases in which one of the phases is dispersed as droplets (the dispersed phase) into the other phase (the continuous phase).[22]

In order to stabilize the interface between the droplets of the dispersed phase and the continuous phase, an amphiphilic molecule is used, which provides the required interface between the two incompatible media. This molecule, called a surfactant (for SURFace ACTive AgeNT) usually surrounds the dispersed phase.[23] When discussing an A/B emulsion, where A and B are two arbitrary and distinct liquids, it is implied that liquid A is the dispersed phase and liquid B is the continuous phase. Thus, for an emulsion that consists of dispersed oil droplets in a continuous water phase, it can be indicated as an O/W emulsion.

1.4.2 Microemulsions vs. Nanoemulsions

There is still a great deal of confusion regarding the key differences between microemulsions and nanoemulsions. Generally speaking, the term "microemulsion" is often used to describe a system of oil, water, and surfactants that is thermodynamically stable. Depending on composition, the microemulsion can be oil continuous or water continuous. It has been mentioned that emulsions go through a bicontinuous phase, but this phenomenon has not yet been evidenced. Also, the dispersed phases can adopt a number of different morphologies such as spheres, cylinders, or sponges.

Nanoemulsions have been referred to as ultrafine emulsions, submicron emulsions, and miniemulsions in the past. Their studies resulted from a growing interest in formulation, pharmaceuticals, and cosmetics for smaller objects that could contain active agents. However, compositionally they are considered to be conventional emulsions that have very small droplets in the dispersed phase. The size threshold can vary greatly. Some consider nanoemulsions to require droplet diameters of less than 100

nm[22, 24] while others consider droplet diameters as large as 500 nm[25] to still fall into the nanoemulsion category. For an oil-water system, nanoemulsions are classified into either O/W or W/O nanoemulsions. Unlike microemulsions that exhibit also bicontinuous phases, nanoemulsions always refer to very small objects in a dispersed phase. Microemulsions are usually prepared by mechanical processes (i.e. high shearing and mixing) and are stable. The main drawback of nanoemulsions was that they were thermodynamically unstable when prepared with conventional methods. They can be synthesized at slightly higher temperatures, but they cannot withstand those temperatures for extended periods of time.

Figure 1 displays the schematic structure of a nanoemulsions droplet. It is quite clear that both O/W microemulsions and nanoemulsions have similar structures with the hydrophilic surfactant head groups assembling on the outside of the oil droplet (into the aqueous phase) and the hydrophobic surfactant tails assembling on the inside of the hydrophobic oil core.[26]

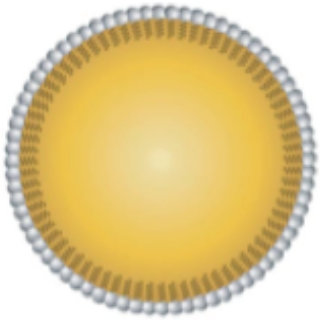

Figure 1: Structure of Nanoemulsion Oil Droplets[23]

1.4.3 Nanoemulsion Preparation

Methods for preparing nanoemulsions can generally be divided into two major categories: high-energy and low-energy methods. High-energy methods involve sonication or homogenizers.[25, 27] One concern with using high-energy methods for

preparing nanoemulsions is the energy consumption and consequential cost, especially for scaling up. Another drawback is that most high-energy methods can be harsh on very fragile molecules. As an example, if one was using a nanoemulsion as a drug carrier, there is a very high probability that a method such as sonication will disrupt or even destroy the drug.[25] Besides, the main drawback in the high-energy preparation methods is the thermodynamic instability of the resulting nanoemulsions that prevents their storage or use.

Low energy preparation methods of nanoemulsions have been reported only a few years ago.[5-6, 28-29] They can be divided into catastrophic phase inversion[30-32] and transitional phase inversion. Catastrophic phase inversion has also been referred to as phase inversion composition (PIC)[33-34] or the emulsion inversion point (EIP)[35] method. Considering an O/W nanoemulsion, the starting phase would be pure oil and surfactants, in which the volume fraction of water would be increased slowly. As the water volume fraction is increased, the system goes through a bicontinuous phase prior to a phase inversion that turns the oil phase, initially the continuous one, into the dispersed phase with the opposite for water. This phenomenon is depicted in Figure 2.[36]

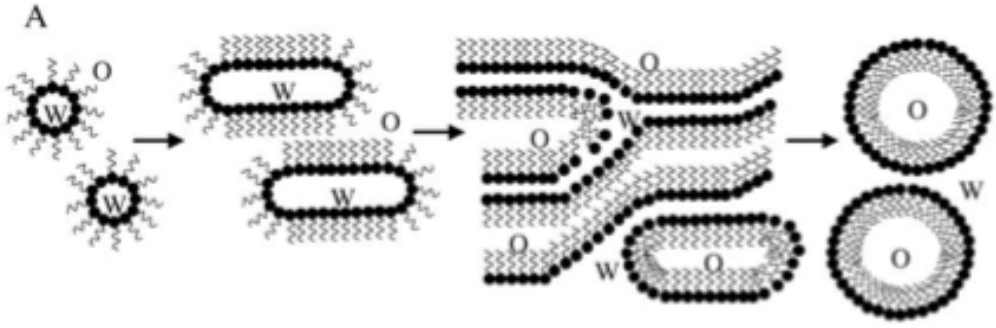

Figure 2: Phase Inversion Composition Phenomenon[36]

The transitional phase inversion technique is also called the phase inversion temperature (PIT) method. This type of method uses rapid changes of temperature to generate small droplets in the dispersed phase. Figure 3 illustrates the impact that a rapid decrease of temperature has on the system. The structuring agent is usually an amphiphilic molecule that contains ethoxy groups (CH_2CH_2O) as hydrophilic moieties. Hydrophilicity of the ethoxy groups results from the hydrogen bonds that the oxygen atom creates with water, but this interaction disappears at high temperature (the transition temperature is called the Cloud Point) and the system becomes mostly hydrophobic. When prepared at temperatures above the Cloud Point and with the suitable choice of amphiphilic molecules and mixture of oil and water, the initial phase is bicontinuous. Once the system is cooled down rapidly, the ethoxy groups become hydrophilic, which changes drastically their interaction with water, resulting in the homogeneous formation of O/W droplets in any point of the reaction. By doing so, the bicontinuous phase is said to "collapse" and thus forms oil droplets making a nanoemulsion. It is also important to note that if the temperature change is not rapid enough, coalescence will predominate and the size of oil droplets will not be homogeneous and phase separation may result.[37]

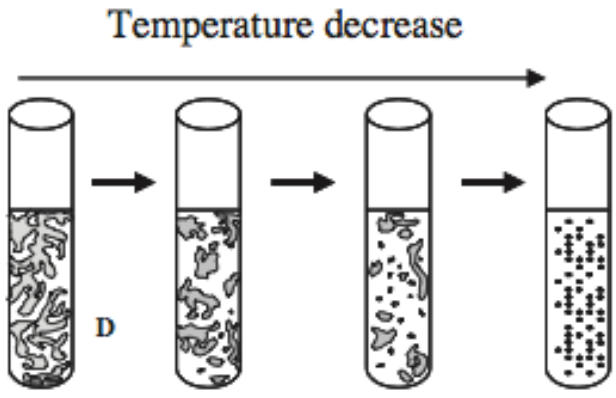

Figure 3: Phase Inversion Temperature Method for Decreasing Temperature[37]

1.4.4 Pure Oil Nanoemulsions

When delving deeper into the area of nanoemulsions, it becomes clear that the topic is quite complex. Liu et al. reported the preparation of oil-in-water nanoemulsions with paraffin oil, Tween80, Span80, and water by using the phase inversion composition (PIC) method. With all of these components come a large number of influential factors on the system.[38-39] One of them is the hydrophilic lipophilic balance (HLB) that is a semi-experimental scale ranging from 1 to 20, which ranks molecules from highly hydrophobic (HLB = 1) to highly hydrophilic (HLB = 20). HLB of surfactants is usually between 4 and 15, as they must demonstrate some amphiphilicity. At this stage, it is worth mentioning that amphiphilic molecules are described either as surfactants (ionic, zwitterionic) or copolymers (i.e. diblock, triblock). We will include all of them under the generic term of surfactant in the following for sake of simplicity. Combining surfactants with different HLB is a way to modify the resulting HLB. Depending on the ratio of each surfactant, the droplet size can vary greatly.[40] If the HLB value is not within a certain range, then the droplet size of the emulsion falls out of the nanometer range.[6] According to the work done by Hessien,[5] decreasing the HLB leads to a reduction in oil droplet size, but Hessien demonstrated that HLB is an apparent controlling parameter of the phenomenon. In this case, Span80 (HLB = 4.3) and Tween80 (HLB = 15) were the surfactants used. An increase in the number of moles of Span80 results in a dramatic increase in the total surface area of the oil droplets.

Another parameter that impacts nanoemulsions is the preparation temperature. Temperature will directly affect the surfactant HLB. For nonionic surfactants, the relationship between HLB and temperature is inversely proportional. Increasing the

temperature by as little as 10 degrees Celsius can cause a decrease in the HLB value of one unit. In conjunction with the HLB, temperature affects the forces that are present and the size of the oil droplets formed. As temperature is increased, the size of oil droplets has been found to decrease, but this phenomenon is only observed during the formation of the nanoemulsion, and temperature has no effect on the oil droplet size after the droplets have been formed.[5]

Another parameter that has an effect on the system is the surfactant concentration. By changing the surfactant concentration, the total interfacial area changes. Liu et al. found that increasing the surfactant concentration made the particle size distribution very narrow.[6] Hessien did a more detailed study on the effect of the surfactant/oil ratio alone on the final size of the oil droplets. It was found that as the surfactant/oil ratio increased, the oil droplet size decreased.[5] This is explained by the fact that higher surfactant concentrations create a higher interfacial surface that can be adapted only for a given volume of the oil phase by creating smaller oil droplets.[41-42]

1.4.5 Pure Wax and Wax/Oil Nanoemulsions

Although it is very common to create nanoemulsions with two liquid phases, Liu et al. have also demonstrated the ability to use paraffin wax/oil mixtures instead of paraffin oil.[7] The paraffin wax is solid at room temperature, which requires the synthesis to be done at an elevated temperature. The PIC method was still used, but the synthesis needed to be performed at the melting temperature of the wax. It is very common to keep the synthesis temperature between 60 °C and 70 °C in order to ensure a homogeneous liquid phase without causing significant evaporation of the water phase. Therefore, the

temperature range when dealing with wax nanoemulsions is much narrower than working with pure oil. Once the synthesis is complete and the final emulsion is allowed to cool, the oil droplets are said to be in a solid phase due to the state of paraffin wax at room temperature.

However, it has been observed that paraffin wax nanoemulsions are only stable for shorter periods of time than oil based nanoemulsions. Backov attributes this phenomenon to something called a jamming transition.[43] The reasoning behind this phenomenon is largely related to the effect that wax density has on the merging or "jamming" of the oil droplets.[44] Wax nanoemulsions generate irregular spheres in the dispersed phase. It is believed that this irregularity and increased surface roughness of the wax allows a jamming transition to occur much more easily.[43]

Destribats et al showed that high-energy methods of creating wax nanoemulsions, was also possible and resulted in similarly successful results.[45] Their procedure involved adding molten wax to a heated water phase while stirring with a homogenizer.

1.5 Mesoporous Silica

Even though the term mesoporous silica referred initially to a range of porosity between 2 and 50 nm, it is now often used as a reference to specific syntheses where micellar systems are combined with silica precursors in order to achieve the preparation of a porous material that exhibits a very well-defined pore size (usually in the 2-10 nm range), potentially with pore tunability, and with a very high surface area (usually > 600 m^2g^{-1}).[46-52] The researchers at Mobil were the first to report ordered mesoporous silica from the family M41S.[53] Porosity was created with a templating mechanism where silica precursors self-assembled around micelles of cationic surfactants, leading to a long-range

order marked by specific X-ray diffraction patterns. The porosity was created after the full reticulation of the silica network by calcination or extraction of the organic phase.

The surfactants that were used by the researchers at Mobil were cationic. Bagshaw et al. were able to use nonionic surfactants whose hydrophobic moiety was a poly(ethylene oxide) (PEO) as the micelle templates, and mesoporous silica synthesized with the use of nonionic PEO surfactants as a template was classified as MSU type silica.[54-55] When considering the synthesis of silica through this type of mechanism there are many parameters that can be adjusted in order to control the final structure. However, the definition of the reaction parameters based on sol-gel methods must adapt to the additional requirements relevant to the structure and stability of soft matter systems. As an example, most of the reactions using metal alkoxides are based on alcohols employed as solvents, but alcohols, which are very good solvents of both hydrophilic and hydrophobic groups, preclude the formation of surfactant-based mesophases, hence micellar-based templating.

One simple synthesis route for creating MSU silica with nonionic PEO-based surfactants was developed with the formation of hybrid micelles, where silica precursors can agglomerate in a diffuse shell around the initial micelle of nonionic surfactants.[56] Unlike all other methods that combine together templating and reaction, the stability of these hybrid micelles allows to control the initiation of the silica condensation by the addition of a condensation catalyst, usually a fluoride that induces silica formation without changing the pH. Once these hybrid micelles had been demonstrated as being adaptive "nanobricks" that could be tuned for the synthesis of mesoporous silica with various pore sizes, they were used in what was called a hybrid micelle concentration

process. This method uses solutions of pre-assembled hybrid micelles that are progressively concentrated in order to achieve the formation of monolithic materials instead of powders, with the ability to embed any additive (i.e. atoms, particles) added beforehand. Unlike the direct preparation of solutions with the same high concentration, which would react before the silica precursor can interact with the surfactant mesophase, the progressive concentration of a diluted system allows one to preserve these independent hybrid micelles without any unforeseen reaction.

In a typical synthesis, the first step is to dissolve a surfactant into water. Once dissolved, the water is then acidified to a pH of approximately 2, which allows for hydrolysis of the silicon alkoxide (TEOS: tetraethyl orthosilicate $Si(OCH_2CH_3)_4$), but prevents silica condensation. The result is a clear solution of hybrid micelles that is left at rest for 12 hours at low temperature to achieve the assembling mechanism between silicate and surfactants. The second main step is to concentrate the hybrid micelles further by evaporating the solvent leaving a highly concentrated hybrid micelle system. The system gelled over time and is processed to provide MSU silica. As mentioned before, this synthesis pathway also allows for entrapment of different elements in the silica matrix. This was achieved by doping atoms into the mixture after the evaporation of solvent (before gelation occurred). Once the gel was formed, the elements added would be trapped inside the structure.[57]

1.6 Templating

There is a large interest in using soft-matter as a structure-directing agent. The process of templating in chemistry refers to the process of integrating a soft-matter template (i.e. organic molecules) in order to synthesize a structure with a continuous

property (i.e. pore size).[10] Templating through the use of micelles and ionic surfactant molecules has been used as a way to synthesize inorganic mesoporous materials with particular physical properties.[58-61] Precursor phases are organized in the micellar structures through surfactant templating.[62] Liquid crystals have also been exploited for templating purposes due the crystal-like arrangement of the molecules and their uniformity. Nanoemulsions are a more recent type of soft matter that have been used to template mesoporous silica. The different templating approaches are based on the type of material that one wishes to synthesize. In terms of mesoporous materials, the different templating approaches provide a different range of pore sizes and can also provide different morphologies. The various templating methods can be used not only to control the final structure of materials, but also to help synthesize more complex and new materials.[63]

1.6.1 Nanoemulsion Templates

These templates can be exploited to synthesize nanoparticles (reactions in dispersed phase), porous materials (reactions in continuous phase), and composites (reactions in both phases). Figure 4 illustrates the resulting structure that forms through the self-assembly of materials in the dispersed and/or continuous phase due to their properties (i.e. hydrophobic vs. hydrophilic).

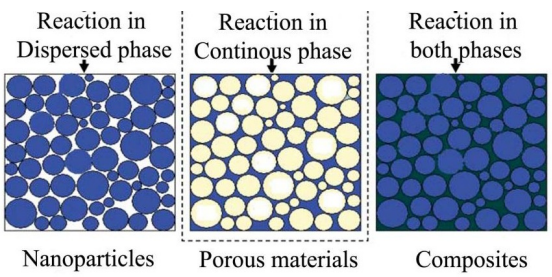

Figure 4: Templating Using Nanoemulsions[64]

In the work done by Hessien, the surfactants that are used are non-ionic and contain PEO (Span80 and Tween80). It is believed that the silica precursors interact with the PEO chains of the nonionic surfactants. Under the appropriate conditions, the silica precursors will self-assemble around the oil droplets through hydrogen bonding with the ethylene oxide.[54] The TEM image shown in Figure 5 depicts a porous structure that is globular in nature, which indicates the silica encapsulating the oil droplets and using them as a template to create a particular porous structure.

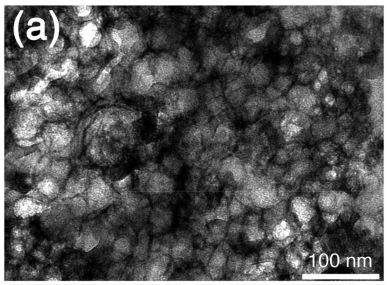

Figure 5: TEM of Porous Silica from Nanoemulsion Templating[59]

In addition to using the oil droplets to create porous structures by surrounding them, a composite was also made by using the oil droplets as carriers for an iron oleate (hydrophobic iron molecules) encapsulated within the oil droplets.[59] Combining this with the silica precursors discussed above, the nanoemulsion is used as a template for nanoparticles and porous structures simultaneously, resulting in a composite structure. Figure 6 shows this composite structure, also referred to as a hierarchical structure.

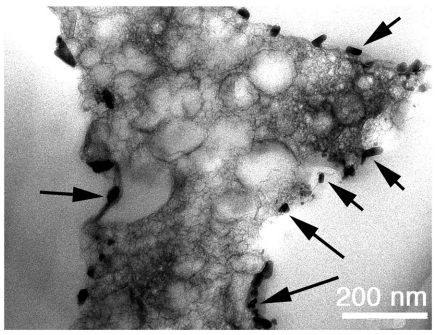

Figure 6: TEM of Composite Structure from Nanoemulsion Templating[59]

1.6.2 Liquid Crystal Templates

Lyotropic liquid crystals (LLCs) are another soft template candidate that is believed to be able to synthesize novel materials.[65] The true LLC templating method is able to synthesize porous materials with very uniform pore size and morphology. It also allows for easy tunability of the pore size through changing the composition of the liquid crystal template. Its structure is known to consist of hexagonally packed tube-like structures.

In the liquid crystal templating mechanism, the inorganic material occupies the continuous solvent (usually water) creating the inorganic layers/walls between the surfactant (cylinder templates). The template is then removed to provide the desired inorganic structure.[65] However there is no literal understanding of what happens during synthesis. The work done by Attard demonstrates the synthesis of hexagonally arranged silica through liquid crystal templating.[65]

Another type of silica that has been synthesized through true liquid crystal templating is of material referred to as class SBA-15. Traditional techniques for synthesizing this type of silica involve using the cooperative self-assembly method. This method starts with acidic conditions, low surfactant concentrations (tri-block copolymers are common), and silica precursors. The liquid crystal phase is formed during

condensation and does not exist as a template prior to the reaction occurring. This type of self-assembly creates a heterogeneous silica structure with mesopores formed from the hexagonal structure and randomly distributed micropores.[66]

The true liquid crystal templating approach, used by Attard et al. to synthesize MCM-41, involves synthesis of the template first and then addition of the silica precursors as illustrated in Figure 4. The research done by Wainwright shows that this method could be used to synthesize hexagonal SBA-15 that has a much more homogeneously uniform mesoporous structure.[66]

In addition to the structure of the liquid crystal template, the type of precursor seems to also have an effect on the final structure of the material. Zhang et al. showed that using the same tri-block copolymer template yet varying the silica precursor at a particular pH affected the final silica structure. The two silica precursors studied were tetramethyl orthosilicate (TMOS) and tetraethyl orthosilicate (TEOS). The use of TMOS as the silica precursor resulted in the formation of highly ordered mesostructures while using TEOS instead produced vesicle or foam structures. The main reason for this structural difference is due to the effect of pH on the silica precursors. Here, a pH of 4.7 was used, which caused a "differentiating effect" between TEOS and TMOS. Under more acidic conditions, one could expect that both would be able to form mesostructures due to what is known as the "leveling effect".[67]

Swollen liquid crystals have also been used to synthesize mesostructured silica. In general, the template of liquid crystals is gel like in nature. Here, the template is a fluidic solution that has a sponge-like structure.[68] The silica precursor that was used in this study is based on a silicate hybrid micelle (arguably another type of template)

consisting of TEOS and a surfactant. This solution is used as the aqueous phase in the liquid crystal. Once silica condensation is induced, the structure is formed. During the reaction, there is confinement within the swollen liquid crystals that expels the surfactant from the silica framework. The resulting silica structure is quite dense. However, the shape is controlled by the sponge-like structure of the swollen liquid crystals as a confinement matrix.[68] Figure 7 shows the resulting sponge-like silica that is formed through this swollen liquid crystal templating process.

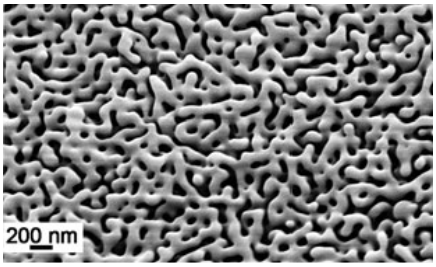

Figure 7: Sponge Like Silica from Swollen Liquid Crystals[68]

Liquid crystal templates are not only restricted to use for synthesis of mesostructured silica. They can and have been used to synthesize metals and metal containing structures. Transition metal salts are often combined with surfactants in a mesophase to produce mesostructured metal oxides, metals salts, and metals that cannot be synthesized using other methods.[69]

Surrendran et al. worked on synthesizing palladium nanoballs through the use of a swollen hexagonal mesophase. The template itself consists of water, surfactant, cosurfactant, and oil. The mesophase has oil-swollen tubes with a surfactant and cosurfactant monolayer covering the tubes. These tubes can be doped with metal salts and are used as nanoreactors. The reduction of the palladium and its confinement in the tubes gives rise to the synthesis of three dimensional porous palladium nanoballs.[70] This process is considered to be a nanomold process.

Lehoux et al. have also looked into oil-swollen surfactant tubes as templates for synthesizing nanostructures made of metals. Similar to the work done by Surrendran, metal salts are used to dope the mesophases and are then reacted through radiolysis. However, this study involves the synthesis of bimetallic nanoballs containing palladium and platinum. The only change that needs to be made from previous works involving the synthesis of single metal nanoballs is the addition of two different metal salts. This shows the versatility and simplicity of synthesizing nanostructured materials through soft templates like liquid crystals. Figure 8 shows the resulting hexagonal cell and the detailed structure of the nanoballs that are synthesized.[71]

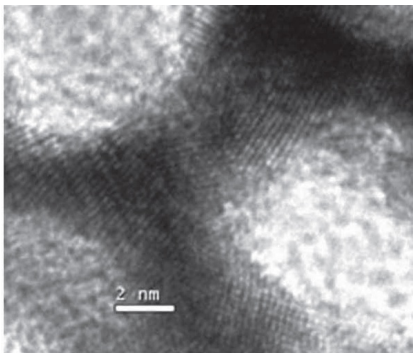

Figure 8: TEM of Hexagonal Mold with Nanowire Interconnections[71]

1.6.3 Surfactant Micelle Templates

Using surfactant micelles as templates is a well-known and quite simple way to synthesize nanostructured materials with specific and desired properties. Ionic surfactants are quite commonly used in order to synthesize ordered mesostructures that are hexagonally packed.[9, 54] However, another interesting pathway is to use nonionic surfactants and their interaction with silica precursors (hydrogen bonding) to synthesize different materials. This mesostructured silica is named MSU-X with the X denoting the type of surfactant that is used for the template.[56, 72-73]

In order to better understand the mechanism that takes place in this templating method, Bagshaw et al. conducted a study where they made a dilute solution of micelles using a surfactant that is known to form spheres. First, the size of the micelles alone was measured. Then, after addition of the silica precursor (in this case TEOS) the size of the particles was measured again. It was concluded that there was an increase in the size of the particles. This indicated that silica precursors assembled on the surface of the PEO chains.[54] This interaction between nonionic surfactants with ethylene oxide and silica precursors generates aggregates referred to as "silicate hybrid micelles".[56] The structure and assembly of components of these hybrid micelles can be seen in Figure 9.

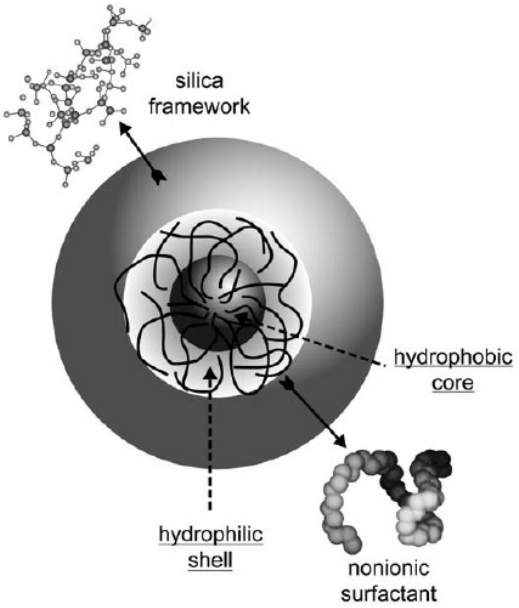

Figure 9: Silicate hybrid micelle Structure[57]

Silicate hybrid micelles alone and the use of simple micelles as templates shows great control in the synthesis of nanostructured materials. Work done by Prouzet et al.[56] showed the ability to synthesize MSU-X type silica with control over the pore size and structure. The interesting property that exists for surfactant micelle templates is their dynamic behavior. Temperature variations cause the size of micelles to either shrink

(lower temperature) or swell (higher temperature). The hybrid micelles containing the silica precursors have been shown to have the same adaptability.[56, 72] This property alone sets this template apart from the nanoemulsions. Liquid crystals have the potential to show some dynamic behavior, but not with the same ease as hybrid micelles. An image taken by SEM of the spherical silica synthesized through this template is shown in Figure 10.

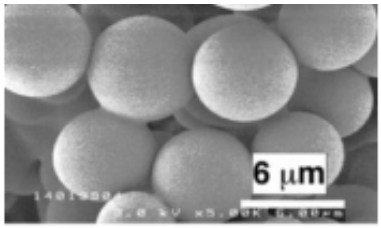

Figure 10: MSU Silica from Hybrid Micelles[8]

In addition, this template is quite versatile in that the shape of the template depends strongly on the type of surfactant that is used. It is even possible to synthesize hexagonal structures through the use of block copolymers (i.e. pluronics) to form the micelle template in solution.[56]

Chapter 2: Characterization Techniques

2.1 Small Angle X-ray Scattering

Small angle x-ray scattering (SAXS) is a powerful characterization technique that can be used to study ordered arrays of atoms. Diffraction peaks are produced based on the constructive interference of X-rays as they pass through the sample. For amorphous and crystalline materials, the size of very small particles (or the surface area) can be determined based on the intensities of the X-rays at very small angles of $2\theta < 5°$.

SAXS is able to determine contrasts from the fluctuations of electron densities over lengths as small as 10 nm. The scattering of the X-ray beams related to the structure of the sample is denoted as a function of q, which is known as the scattering vector and is the difference between the incident and scattered wave vectors in units of nm^{-1}. In order to get a best estimate of distance between nano-objects in a particular system, it is very common to use the following relationship where d represents the distance.[74-75]

$$d = \frac{2\pi}{q} \tag{1}$$

From Bragg's law it is known that $n\lambda = 2d\sin\theta$ where n is the refractive index, λ is the wavelength of the incident beam, and θ is the angle between the incident beam and the scattered beams. By taking n to equal 1 this relationship can be rearranged for d and substituted into the Bragg equation to yield the relationship shown in (2).

$$q = \frac{4sin\theta}{\lambda} \tag{2}$$

The SAXSess system by Anton Paar will be used to perform measurements with the SAXSquant and OptiQuant software. A 2.2 kW copper anode having a wavelength of 1.54 Å and an angle range of 2θ from 0° to 40° will be used.

2.2 Nitrogen Adsorption/Desorption Isotherm

Nitrogen adsorption and desorption isotherms are useful for characterizing the pore size distributions and surface area of porous materials.[74] There are many different models that are used when analyzing nitrogen isotherm plots, which all depend on the pressure range being looked at. For the calculation of the surface roughness, Equation 3 can be used.

$$\theta = \mathrm{K}\left[\log\left(\frac{P_0}{P}\right)\right]^{-v} \tag{3}$$

where θ is the relative adsorption for normalization of the curve using the highest adsorption value, K is a constant, $v = 3 - D_s$, P_o and P are the are the equilibrium vapor and partial pressures respectively, and D_a is the surface fractal dimension.[75] To easily convert the equation in a way that D_s is more easily obtained, the logarithm of each side is taken as shown in Equation 4.[75]

$$\log(\theta) = \log(K) - v \cdot \log\left[\log\left(\frac{P_0}{P}\right)\right] \tag{4}$$

To determine the surface area of the materials, one must employ the Brunauer, Emmett, and Teller (BET) theory. It is an extension of the Langmuir theory with the difference that it can be applied for more than one layer of adsorbate. Multiple layers

will be adsorbed as the pressure increases. The relationship that is used for the BET model is the following:

$$\frac{n}{n_{mon}} = \frac{C}{1-\frac{P}{P_0}} \cdot \left(1 + \left(\frac{P}{P_0} \cdot (C-1)\right)\right) \cdot \frac{P}{P_0} \quad (5)$$

where n is the number of adsorbed moles per unit area, n_{mon} is the number of moles adsorbed for a full monolayer per unit area, and C is approximated by the relationship $e^{\frac{Q_1 - Q_i}{RT}}$ with Q_1 being the heat of adsorption for the first layer, Q_i being the heat of condensation of the liquid and R and T being the gas constant and temperature respectively.[76]

2.3 Scanning Electron Microscopy

Scanning electron microscopy will be used to investigate the shape, size, composition, and surface of the materials that will be prepared. SEM can be visualize pores in a silica matrix. Analysis of gold sputtered samples can provide three-dimensional images with high resolution.

2.4 Dynamic Light Scattering

Dynamic light scattering is a very useful technique that can be used to determine the hydrodynamic diameter of small particles in solution. Based on the Brownian motion of particles in solution, light will scatter differently over time. The diffusion coefficient is then used to determine the hydrodynamic diameter of the particle using the Stokes-Einstein equation shown below where k_B is the Boltzmann constant, T is the temperature

in Kelvin, η is the viscosity of the solvent at the given temperature, and D_h is the hydrodynamic diameter.

$$D = \frac{k_B T}{3\pi\eta \mathrm{D}_h} \tag{6}$$

The instrument used was a Cordouan DL 135 Particle Size Analyzer with a 65 mW monomode red laser (λ = 658 nm). Two models were used to fit the results: a single size cumulant fit and a Padé-Laplace fit. The autocorrelation function for every scan was fitted with the Padé-Laplace model. The statistical size distribution was deduced from sizes obtained for every single scan with the average size of all scans being taken.

2.5 Fluorescence Spectroscopy

Fluorescence spectroscopy is used to determine dynamic and structural information at the nanometer scale on macromolecules and their supermolecular assemblies. Steady-state fluorescence measurements were carried out to obtain the fluorescence spectra with a Photon Technology International (PTI) LS-100 steady-state fluorometer equipped with an Ushio UXL-75Xe xenon arc lamp and a PTI 814 photomultiplier detection system.[77]

Fluorescence decays were carried out with an IBH time-resolved fluorometer fitted with a 340 nano-LED light source. Filters were applied to eliminate background and light scattering effects in order to fit the decays. A sum of exponentials, such as the one shown in Equation 7, was used to fit the fluorescence decay curves

$$i(t) = \sum_{i=1}^{n_{exp}} a_i \cdot e^{\left(-\frac{t}{\square_i}\right)} \tag{7}$$

where n_{exp} represents the number of exponentials used, a_i the amplitude of the i^{th} exponential, and τ_i is the decay time of the i^{th} exponential.[77]

2.6 Fourier Transform Infrared Spectroscopy

Fourier transform infrared spectroscopy (FTIR) is a technique that is used to confirm the molecular structure of materials. The absorption of IR light by molecules at well-defined frequencies results in patterns reflecting the energies associated with particular molecular motion in the molecule. The instrument used was a Brucker Tensor 27 spectrometer (OPUS software). Spectra were recorded from 400 to 4500 cm^{-1} using 16 scans. Samples were prepared by mixing *x* grams of sample with y grams of KBr (Fisher Scientific) to generate a pellet that was then scanned.

2.7 X-ray Powder Diffraction (XRD)

X-ray powder diffraction (XRD) is a technique that is used to determine crystal structures and identify different crystalline materials based on the diffraction peaks that are obtained. The interplanar distance, *d*, can be obtained by using the Bragg relationship show in in Equation 8 where λ is the X-ray wavelength and 2θ is the angle of incidence of the X-ray beam.

$$\lambda = 2dsin\theta \quad (8)$$

XRD patterns were obtained using a Bruker D8-ADVANCE powder diffractometer operating at 40 kV using Cu Kα radiation (λ = 1.5405 Å) operating from 2θ values of 10° to 80°

Chapter 3: Structure and Dynamics of Silicate Hybrid Micelles

The synthesis used in this research was based on earlier work reporting on the structure of silicate hybrid micelles used for the synthesis of mesoporous silica.[56] The present study extends the previous results, significantly by generalizing to a broad range of surfactants compared to the original study that focused on a single surfactant.

3.1 Experimental Methods

In a typical synthesis for silicate hybrid micelles, 2 x 10^{-3} mol of a nonionic ethylene oxide based surfactant was dissolved in 100 mL of water (pH 2). After complete dissolution, 20 x 10^{-3} mol TEOS was added drop by drop under stirring at 500 rpm. The solution turned cloudy immediately after the addition of TEOS. The solution was left to stir until it turned clear, indicating the hydrolysis of the TEOS. This solution was left overnight in the refrigerator to age.

For DLS studies, 20 scans were performed at every temperature (from 15 to 65 °C at 10 °C intervals). The amount of surfactant was kept constant at 2 x 10^{-3} mol, while the amount of TEOS was set to be either 0.0 mmol, 20 mmol (TEOS/surfactant = 10) or 40 mmol (TEOS/surfactant = 20), The naming convention used for these samples is X-DLS-N, where X is the surfactant name and N is the TEOS/surfactant molar ratio.

Silicate hybrid micelles prepared for fluorescence studies used 2 x 10^{-3} mol Tergitol 15-S-12 as the surfactant. The TEOS/surfactant molar ratios used were 0, 5, 10, and 15. These solutions of hybrid micelles were diluted with water (pH 2) to produce a series of 10 mL samples with different concentrations. Pyrene was added to these samples as a probe for fluorescence measurements. Since the amount of pyrene required was very small, the amount to be added was obtained by first diluting pyrene in THF

until a specific absorbance was obtained as determined by UV-Visible spectrometry. The concentration in pyrene was deduced from the absorbance of the solution. A given volume of this solution was extracted, and THF was evaporated under nitrogen bubbling, leaving the suitable amount of pyrene behind. This amount was then combined with a diluted aqueous solution of silicate hybrid micelles and left to shake for 3 hours to ensure full transfer of pyrene into the micelles.

Two types of fluorescence analyses were conducted: steady-state and time-resolved fluoresence. For steady-state fluorescence, a solution of pyrene in THF having an absorbance of 0.2 was prepared. From this solution, 0.5 g was taken out and the THF was evaporated leaving behind the pyrene. This amount of pyrene was combined with dilutions of four different aqueous solutions of silicate hybrid micelles prepared with different TEOS/surfactant molar ratios. Each solution was studied at 10 different dilutions of hybrid micelles. These samples are refered to as T15-S-12/FSS/N/c, where *N* is the TEOS/surfactant ratio and *c* is the surfactant concentration. The concentrations with respect to the surfactant used for the steady state analysis were 0.04 mM, 0.047 mM, 0.062 mM, 0.10 mM, 0.12 mM, 0.14 mM, 0.18 mM, 0.21 mM, 0.28 mM, and 0.84 mM.

For time-resolved fluoresence, the surfactant concentration for the four aqueous solutions of silicate hybrid micelles was fixed at 0.52 mM and various amounts of pyrene were added. A 0.13 mM solution of pyrene in THF was initially prepared, with its concentration determined by UV-Vis absorbance. Increasing amounts of this solution (0.083 g, 0.166 g, 0.249 g, 0.332 g, 0.498 g, 0.664 g) were evaporated to sample different amouns of pyrene, which were added to the aqueous solution of silicate hybrid micelles.

These samples are referred to as T15-S-12/FLT/N/0.52 with *N* representing the TEOS/surfactant ratio.

3.2 Silicate Hybrid Micelle Analysis

The structure and dynamics of silicate hybrid micelles have been previously studied using one type of alkyl (PEO) surfactant. This chapter extends and validates the previous results to a broader range of surfactants, and it probes the differences between different types of non-ionic surfactants.

These results are important to increase our knowledge on the type of nonionic surfactants used to synthesize mesoporous silica, and how the features of the final material was affected by the different structures of the initial silicate hybrid micelles. The surfactants that were chosen for study were Tergitol 15-S-12 (d = 0.993, M_w = 740 g, $C_{12\text{-}14}H_{25\text{-}29}O[OC_2H_4]_xH$), Tergitol 15-S-30 (d = 1.055, M_w = 1520 g, $C_{11\text{-}15}H_{23\text{-}31}O(OC_2H_4O)_xH$), Tergitol NP-10 (d = 1.060, M_w = 645 g, $C_{15}H_{24}O(C_2H_4O)_n$), Tween20 (d = 1.095, M_w = 1230 g, $C_{18}H_{34}O_6(C_2H_4O)_n$), Brij98 (d = 1.070, M_w = 1150 g, $C_{18}H_{35}(OC_2H_4)_{20}OH$), Brij35 (d = 1.060, M_w = 1198 g, $(C_2H_4O)_nC_{12}H_{26}O$), and P123 (d = 1.040, M_w = 5800 g, $HO(CH_2CH_2O)_{20}(CH_2CH(CH_3)O)_{70}(CH_2CH_2O)_{20}H$). The silicate hybrid micelles prepared with these surfactants were studied by DLS between 15 ºC and 65 ºC with measurements taken every 10 ºC intervals. Once the sample reached 65 ºC, the silicate hybrid micelles were cooled back down to 15 ºC and measurements were again taken every 10 ºC intervals. The average value of the hydrodynamic diameter of the scans at each temperature were plotted to provide the trends. Hydrodynamic diameter values for individual scans at each temperature were also plotted, with "x's" used for the silicate hybrid micelles and "+'s" being used for pure micelles. There is a 1% error

associated with the average values unless otherwise indicated. Some samples could not be studied at high temperatures because of the silica condensation reaction being initiated by temperature, despite the absence of catalyst (NaF) usually used for these syntheses.[56]

3.2.1 Temperature Dependent Structural Evolution: the X-DLS-N series

Silicate hybrid micelles were first studied in detail using Tergitol 15-S-12 as the surfactant. Figure 11 shows the evolution of the hydrodynamic diameter of T15-S-12-DLS-10, deduced from the diffusion coefficient, as a function of temperature.

We observe that the size of the silicate hybrid micelles is noticeably larger than that of the surfactant micelles alone, but both populations are monodisperse. For example, at 15 ºC, T15-S-12-DLS-0 has a hydrodynamic diameter of 8 nm (± 0.1 nm), and T15-S-12-DLS-10 a hydrodynamic diameter 11 nm (± 0.1 nm). This observation confirms that the addition of TEOS and its further hydrolysis does create micellar objects that integrate the silicates resulting from the hydrolysis. This was described previously as the formation of a diffuse silicate palisade interacting with the hydrophilic PEO shell.

The second observation confirms the previous preliminary results regarding the similar evolution of silicate hybrid micelles, compared with pure micelles. It is well known that nonionic micelles increase in size with temperature as a result of an increasing hydrophobicity of the PEO chains with temperature.[56] Our analyses demonstrate that the silicate hybrid micelles adopt the same adaptive evolution. T15-S-12-DLS-10 increases from 11 nm (± 0.1 nm) at 15 ºC to 19 nm (± 0.2 nm) at 65 ºC. In addition, the dynamic behavior is retained when the sample is cooled down, with the hydrodynamic diameter getting back to a smaller value and still following the same size trends as that of the heating curve. When T15-S-12-DLS-10 is cooled back down to 15

ºC, the original hydrodynamic diameter of 11 nm (± 0.1 nm) is once again obtained. This demonstrates that the silicate hybrid micelle responds to temperature in the same manner as the pure micelles do, which means that the surfactant is still controlling the structure and dynamics of this hybrid object.

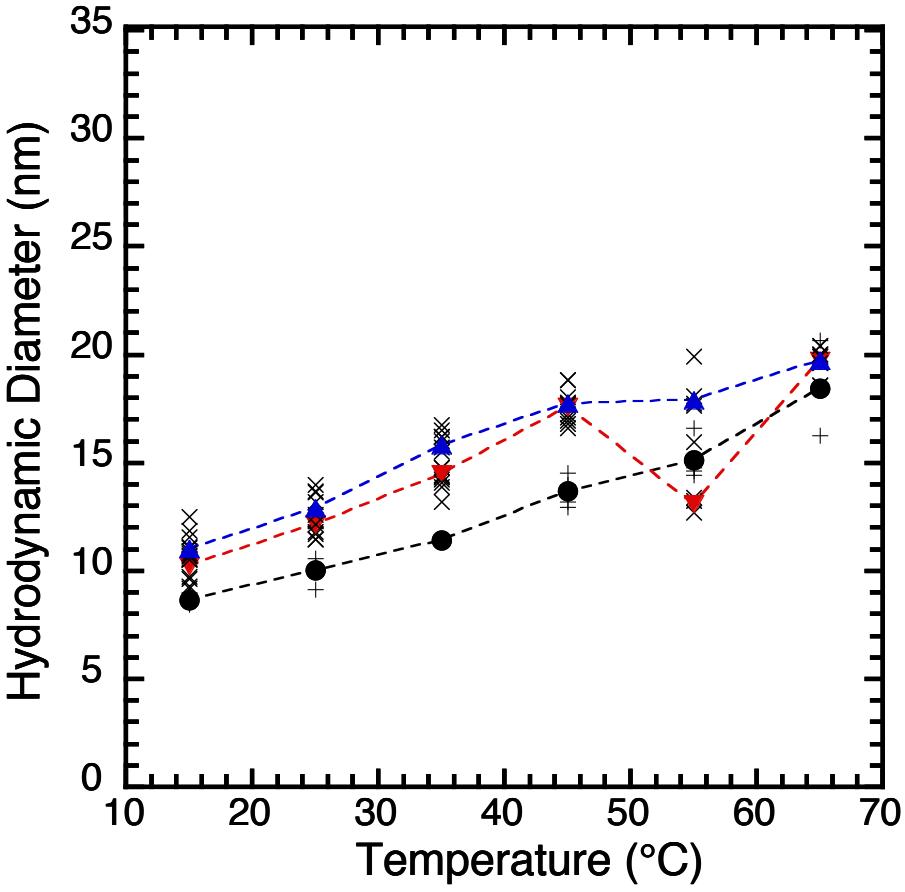

Figure 11: Evolution of hydrodynamic diameter as function of temperature of (●) T15-S-12-DLS-0 ▼heating of T15-S-12-DLS-10, and ▲cooling of T15-S-12-DLS-10.

As it was demonstrated previously that the amount of TEOS used to form the silicate hybrid micelles affects the initial hydrodynamic diameter,[56] we tried to understand if an increased amount of TEOS would affect the temperature dependence of these hybrid micelles.

Figure 12 displays the temperature dependence of T15-S-12-DLS-20. We observe that the initial hydrodynamic diameter at 15 ºC is 12 nm (± 0.1 nm), which is slightly larger than the T15-S-12-DLS-10 sample. However, unlike T15-S-12-DLS-10, the variation of the hydrodynamic diameter with temperature is limited: the hydrodynamic diameter of T15-S-12-DLS-20 heated up to 65 ºC is only 14 nm. We conclude that the structure of the hybrid micelle as the amount of silicate increases is still dynamic and able to adapt to temperature changes, but within a smaller range, as a result of the increasing stiffness created by a thicker silicate layer. The adaptive structure is confirmed with the cooling ramp where the hydrodynamic diameter recovers its initial value of 11 nm (± 0.1 nm).

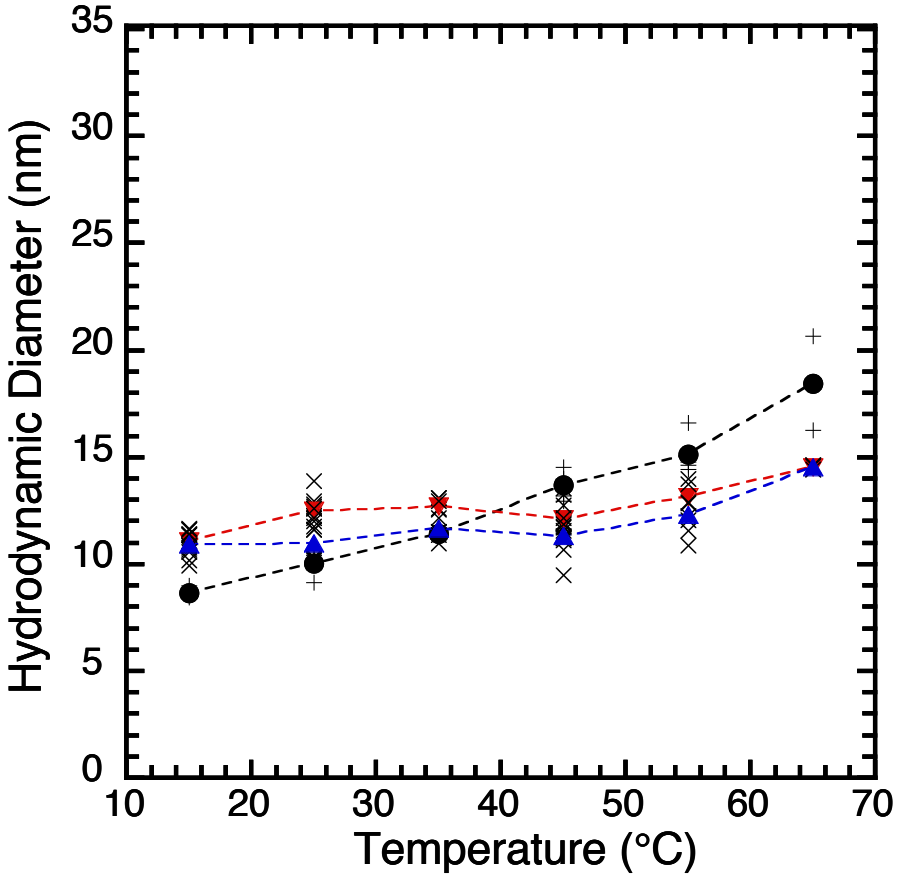

Figure 12: Evolution of hydrodynamic diameter as function of temperature of (●) T15-S-12-DLS-0 ▼heating of T15-S-12-DLS-20, and ▲cooling of T15-S-12-DLS-20.

These analyses were reproduced with Brij35, which has a higher molecular weight than Tergitol 15-S-12, and showed easier adaptability at higher TEOS concentrations. Figure 13 displays the heating and cooling behaviour of Brij35-DLS-10. This sample shows only a slight increase in hydrodynamic diameter from 16 nm (± 0.2 nm) at 15 ºC to 19 nm (± 0.2 nm) at 65 ºC. This increase in hydrodynamic diameter is not as large as for T15-S-12-DLS-10, but it still follows the trends of Brij35 pure micelles, with a diameter increasing from 9 nm (± 0.1 nm) at 15 ºC to 14 nm (± 0.1 nm) at 65 ºC. Upon cooling Brij35-DLS-10, the evolution of the hydrodynamic diameter

displays the same reversible trend, with an evolution back down to 16 nm (± 0.2 nm) at 15 ºC.

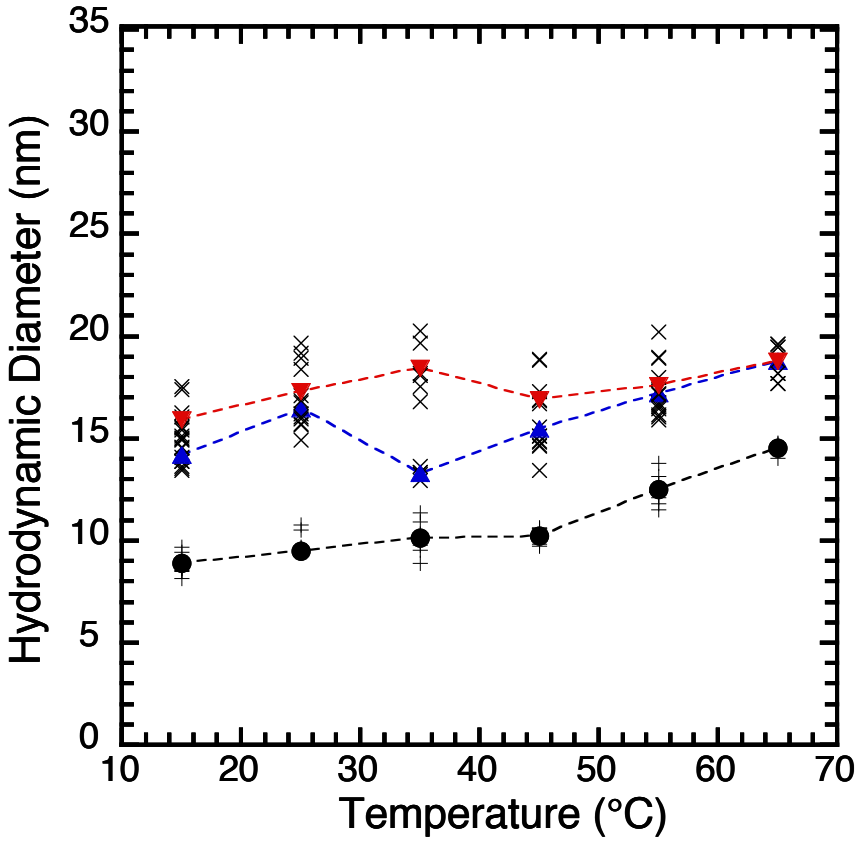

Figure 13: Evolution of hydrodynamic diameter as function of temperature of (●) Brij35-DLS-0 ▼heating of Brij35-DLS-10, and ▲cooling of Brij35-DLS-10.

Increasing the silicate ratio (Brij35-DLS-20) shows that the dynamic behavior is still observed for Brij35, which is opposite of Tergitol 15-S-12. Figure 14 shows the hydrodynamic diameter of Brij35-DLS-20 increases from 13 nm (± 0.1 nm) at 15 ºC to 20 nm (± 0.2 nm) at 65 ºC, which is totally reversible.

The T15-S-30-DLS-N series showed a similar dynamic behaviour with temperature dependent change for both TEOS/surfactant ratios (N= 10 and N = 20) (See Appendix A).

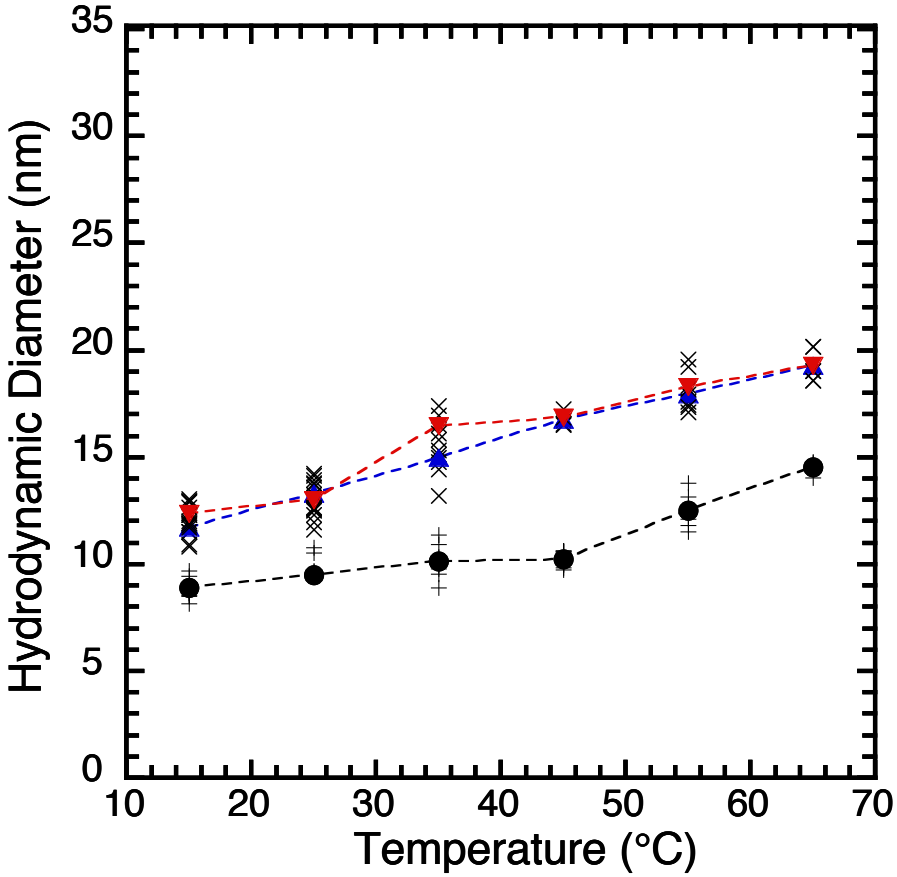

Figure 14: Evolution of hydrodynamic diameter as function of temperature of (●) Brij35-DLS-0 ▼heating of Brij35-DLS-20, and ▲cooling of Brij35-DLS-20.

Our analyses show that the influence of adding silicate depends on the nature of the non-ionic surfactant or copolymer. For example, hybrid micelles can be prepared with Tween20 and lead to the same type of mesoporous silica as for Tergitol 15-S-12.[56] However, the DLS analysis of hybrid micelles (Tween20-DLS-10 series) reveals a different influence of silicate (Figure 15). Only a slight increase in size is observed upon TEOS addition with a diameter varying from 12 nm (± 0.1 nm) at 15 ºC to 17 nm (± 0.2 nm) at 65 ºC compared to the pure micelles (10 nm at 15 ºC to 16 nm at 65 ºC). The smaller difference results from the different distribution of EO groups, distributed in 4 different sites of the molecule, compared with the alkyl-PEO surfactants like Tergitol 15-

S-12 where the EO groups are on the same chain. It results probably from this different structure that the swelling influence of the silicate groups is "diluted" throughout the micelles instead of forming an external palisade.

Adding more silicate confirms the partial loss of structural dynamics and Tween20-DLS-20 shows a similar evolution with a lower evolution with temperature than T15-S-12-DLS-20 (Appendix A). There is no noticeable evolution of the hydrodynamic diameter observed until the maximum temperature of 65 ºC is reached. As an overall behaviour, the silicate hybrid micelles follow the same type of trends as the surfactant micelle alone, which indicates the template retaining dynamic behaviour even in the presence of TEOS.

The other samples that show the same resistance to change with temperature are those prepared with Tergitol 15-S-30 and Brij98 (Appendix A).

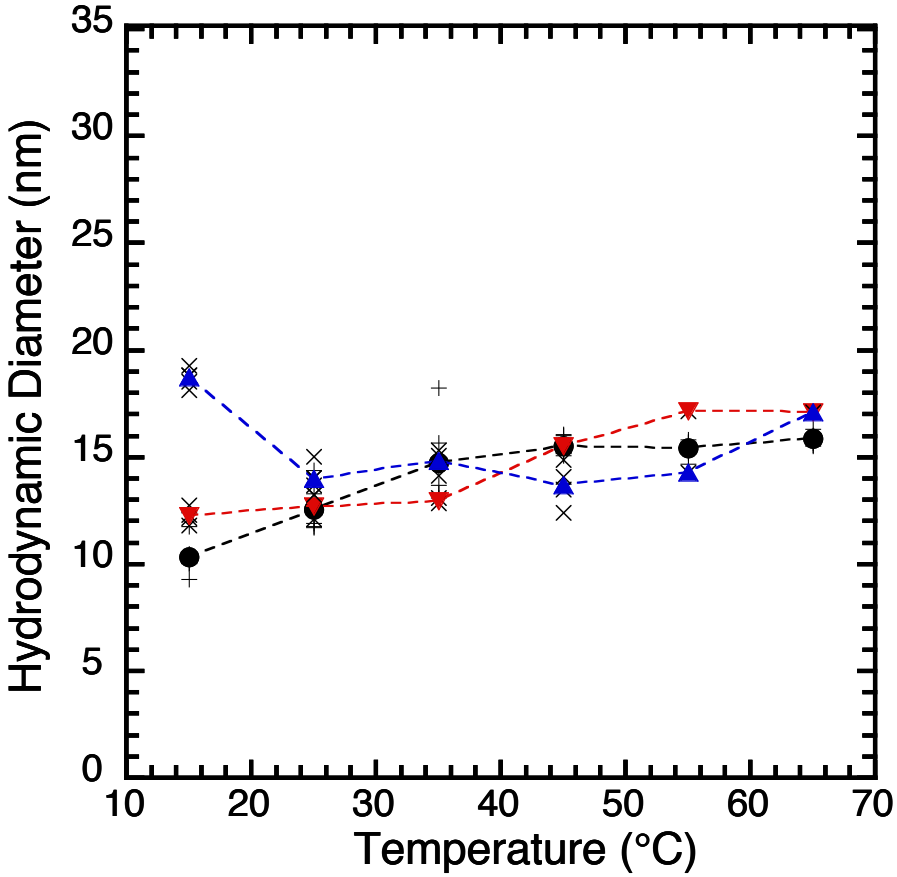

Figure 15: Evolution of hydrodynamic diameter as function of temperature of (●) Tween20-DLS-0 ▼heating of Tween20-DLS-10, and ▲cooling of Tween20-DLS-10.

Tri-block PEO-PPO-PEO copolymers display another molecular structure, with the combination of two PEO chains connected by a hydrophobic PPO linker. Pluronic 123 is one of the most common copolymers used for the synthesis of mesoporous silica since its report for the preparation of hexagonal SBA-15 materials by the Stucky group in highly acidic medium.[49] It was demonstrated that similar well-ordered hexagonal structures could be obtained by using mild acidity and starting from silicate hybrid micelles, if the synthesis temperature was optimized.[19] This temperature-dependent structure was assigned to the higher stiffness of the micelles resulting from the self-assembly of these (EO_{20}-PO_{70}-EO_{20}) copolymers.

Figure 16 shows how P123-DLS-10 changes as a function of temperature with a 3% error associated to the average values. The hydrodynamic diameter of P123-DLS-0 at 15 ºC is surprisingly high (26 nm ± 0.9 nm), but we observe a large statistical distribution of results. These PPO-based copolymers possess a critical micelle temperature (CMT) below which the PPO groups are too hydrophilic, resulting in the molecules being fully dissolved. This CMT is close to 10 ºC, which means that micelles at 15 ºC are not strongly structured and look probably more like loose aggregates than well-defined micelles. This is confirmed with the results at 25 ºC, displaying a smaller diameter (16 nm ± 0.5 nm) and a narrower distribution of values. If we take this 25 ºC value as a starting point, we observe that the size of pure micelles is not significantly changing with temperature. The heating and cooling trends of P123-DLS-10 confirms the same size stability, except at 65 ºC, where a drastic increase of the micelle size from 20 nm (± 0.6 nm) to 40 nm (± 1.2 nm) is observed. This brutal size evolution cannot result from silica condensation because it is reversible.

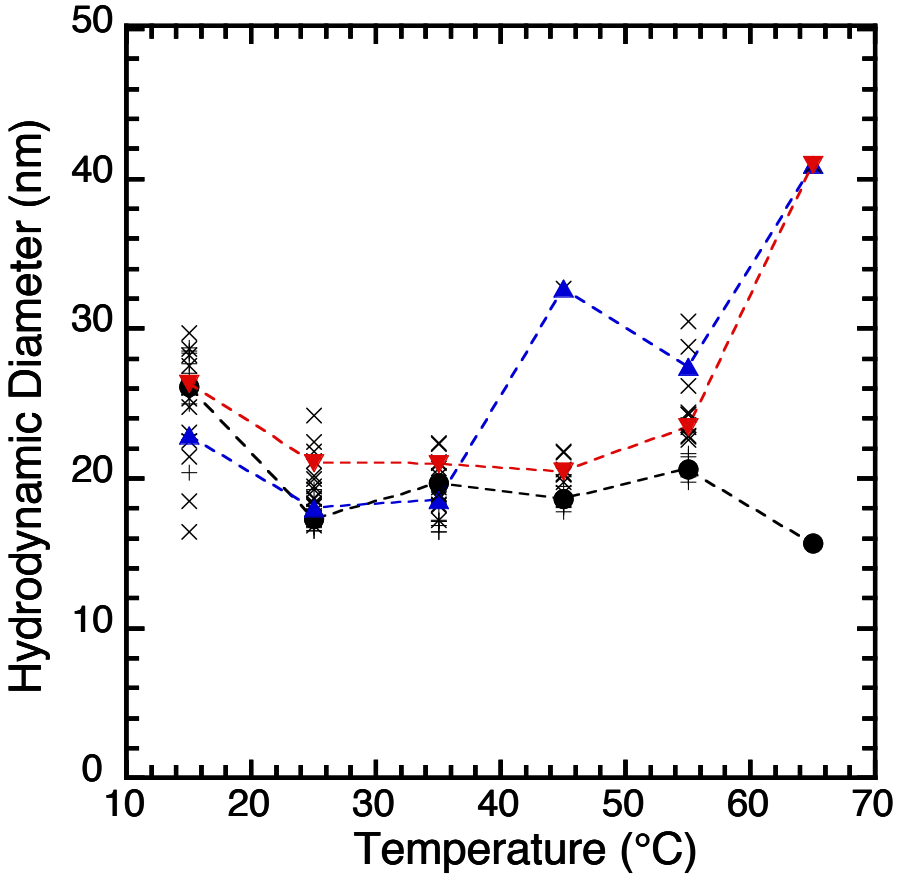

Figure 16: Evolution of hydrodynamic diameter as function of temperature of (●) P123-DLS-0 ▼heating of P123-DLS-10, and ▲cooling of P123-DLS-10.

Figure 17 shows the trends observed for P123-DLS-20. If we take again as a starting point the value of the hydrodynamic diameter at 25 ºC, we still observe the same evolution as P123-DLS-10 micelles retain a fairly constant size until the temperature is significantly increased. The threshold here is at 45 ºC and the hydrodynamic diameter of the silicate hybrid micelles varies from 30 nm (± 0.9 nm) to 90 nm (± 2.7 nm) at 65 ºC. Still, this evolution is fully reversible and the hybrid micelles recover their initial diameter when cooled down to 35 ºC.

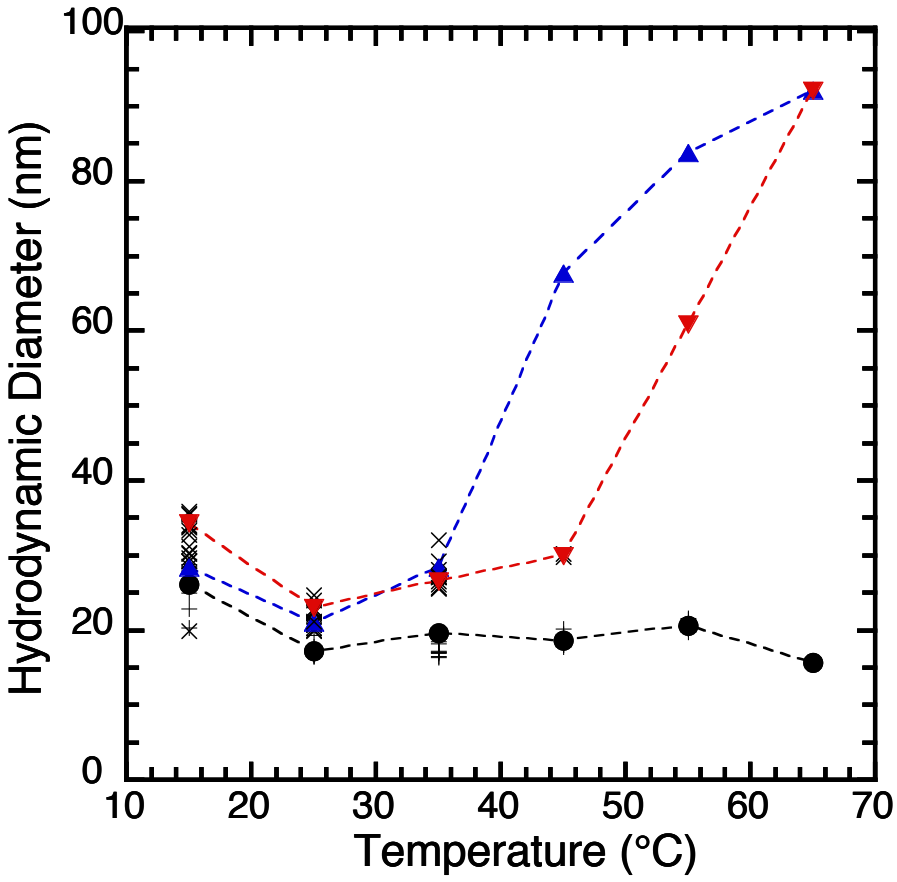

Figure 17: Evolution of hydrodynamic diameter as function of temperature of (●) P123-DLS-0 ▼heating of P123-DLS-20, and ▲cooling of P123-DLS-20.

3.2.2 Steady State Fluorescence of Tergitol 15-S-12 Silicate Hybrid Micelles

We carried out steady-state fluorescence measurements to probe the influence of TEOS on the formation and structure of micelles. Only silicate hybrid micelles synthesized with Tergitol 15-S-12 as the copolymer were used for these fluorescence measurements. Figure 18 shows the evolution of the I1/I3 ratio with concentration in micelles (we used the surfactant concentration as a reference) for the T15-S-12/FSS/N/c series. This evolution allows us to follow how polar the environment of pyrene is (I1/I3 varies from 1.87 in polar water to 0.66 in aploar cyclohexane). The I1/I3 ratio decreases as the concentration in surfactant increases up to a 0.11 mM concentration beyond which

the I1/I3 ratio remains constant The results demonstrate that more pyrene molecules, initially dissolved in water (the polar environment), enter the micelle (the non polar hydrophobic environment) as the surfactant concentration increases. For a concentration of 0.11 mM, all pyrene has entered the core of the micelles, and this threshold concentration does not vary with TEOS/surfactant ratio. We conclude from this analysis that the presence of the silicate shell does not disturb the formation of micelles.

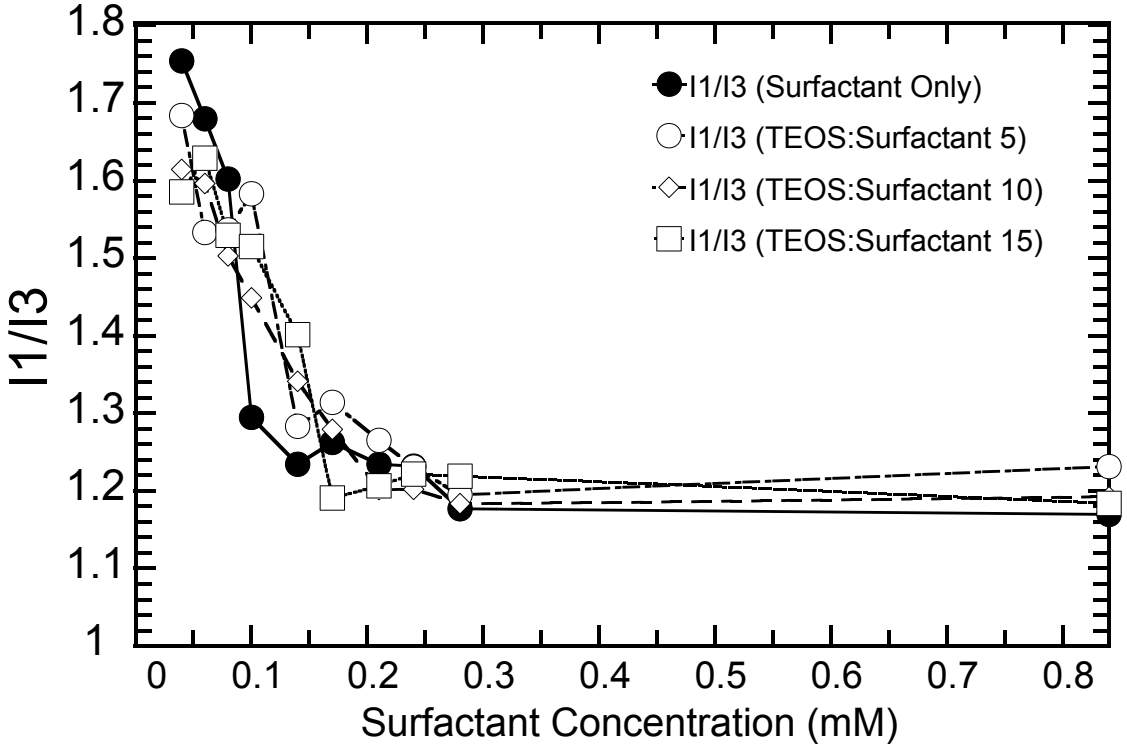

Figure 18: I1/I3 ratios calculated for T15-S-12/FSS/N/c series for all concentrations.

Steady-state fluorescence measurements also provide the relationship between the excimer (IE) resulting from dimer formation, and monomer (IM) intensities through the IE/IM ratio, which helps determine the critical micelle concentration (Figure 19). Figure A 8 in Appendix A displays the fluorescence spectra for the different surfactant concentrations. The IM value is the average intensity between 468 nm and 474 nm and the IE value is the average intensity between 500 nm and 530 nm. The IE/IM ratio,

initially low, increases with increasing surfactant concentration until a maximum value is reached. The excimer is initially formed in the core of the few micelles present. Adding more surfactant generates more micelles that draw more pyrene. In leading to increased excimer formation. The maximum of the curve corresponds to the critical micelle concentration (cmc). As the surfactant concentration is increased further, the IE/IM ratio gets smaller as the few pyrenes available distribute themselves which prevents pyrene excimer formation. The maximum IE/IM ratio for the surfactant alone is 0.11 mM and the same cmc is obtained for the silicate hybrid micelles of all TEOS/surfactant ratios (0.12 mM). These measurements confirm the previous observation, with a cmc undisturbed by the presence of silicates.

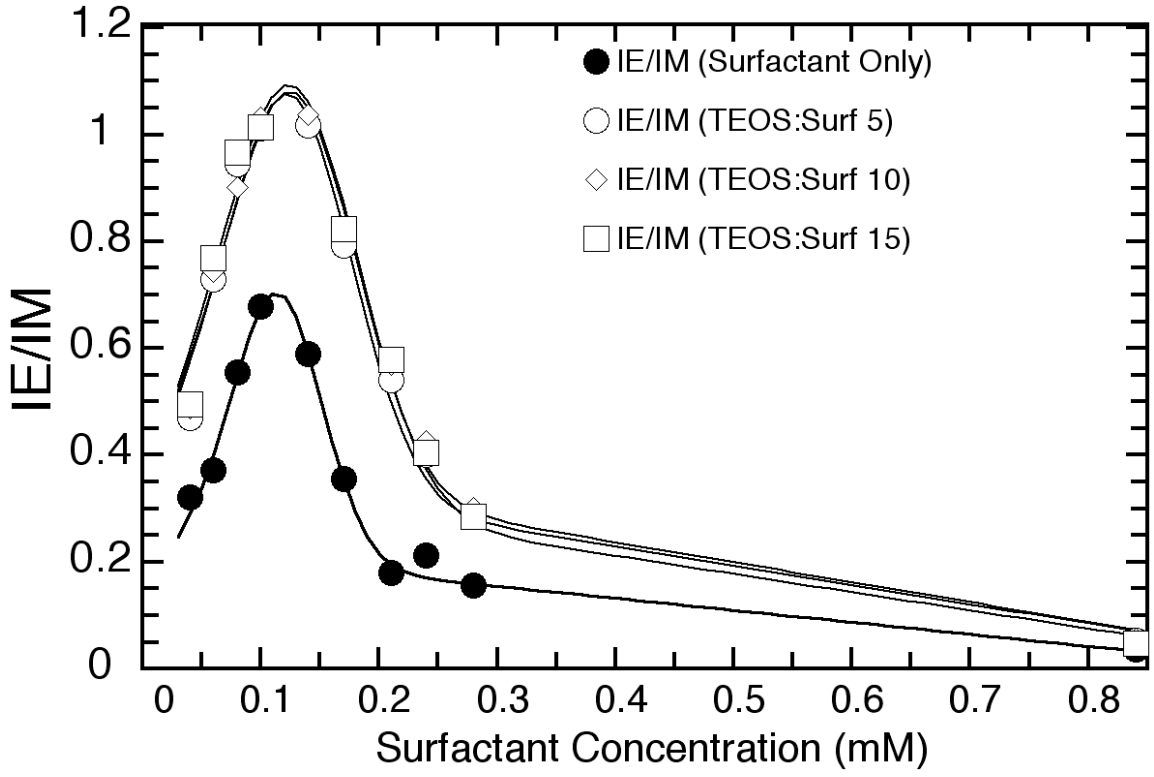

Figure 19: IE/IM Ratio at Various TEOS/Surfactant Ratios

3.2.3 Lifetime Fluorescence of Tergitol 15-S-12 Silicate Hybrid Micelles

Lifetime studies were performed on silicate hybrid micelles in order to determine the effect of TEOS on the micelle aggregation number. To determine the aggregation number, we first look at the relationship in Equation 9 where $[Py^*]$ is the concentration in excited pyrene, $[Py^*]_0$ is the initial concentration in excited pyrene, $<n>$ is the number average degree of polymerization, k_q is the fluorescence quenching rate, and t is the time.

$$[Py^*] = [Py^*]_0 \, e^{[-t/\tau_{py} - <n>(1-e^{-kqt})]} \tag{9}$$

Using the fits from this equation, we can determine and plot $<n>$ versus $[Py^*]$ to get a linear equation. The slope of this line corresponds to the following equation, from which we can deduce the aggregation number. Tables A 1 and A 2 (Appendix A) displays some of the relevant parameters used for these calculations.

$$\frac{N_{agg}}{[surfactant] - cmc} \tag{10}$$

The aggregation number for T15-S-12/0/0.52 was determined to be 98 ± 2. When TEOS was added, the aggregation number increased with aggregation numbers for T15-S-12/5/0.52, T15-S-12/10/0.52, and T15-S-12/15/0.52 being 103 ± 2, 108 ± 2, and 107 ± 4 respectively. This increase in aggregation number indicates that in the T15-S-12/0/0.52 sample, there may be an interaction between micelles causing exchange of pyrene, which diminishes as soon as silicate is present.

3.3 Model of the Silicate Hybrid Micelle System

Silicate hybrid micelles show changes of their hydrodynamic diameter as a function of temperature. Although different surfactants exhibit a different behavior, the structure itself still consists of a micelle as the core and a silicate layer as the inorganic

shell surrounding it, whose thickness can be deduced by the increase in size from the initial micelle without TEOS. We observe that the types of surfactants show different variations with temperature. However, the type of behavior that is observed for the surfactant micelles over the temperature gradient is similar to that of the silicate hybrid micelles synthesized using the same surfactant. This indicates that the silicate layer formed around the micelle core is not rigid enough to prevent swelling of micelles. Some stiffness is observed as the amount of silicate, hence the thickness of the silicate layer increases, which partially or totally prevent the temperature-dependent size evolution of hybrid micelles, depending on the nature of the copolymer used.

Fluorescence studies demonstrated that the silicate layer had an effect on the interaction of the particles in solution, but does not influence the formation of the micelles. The critical micelle concentration is not affected by the presence of TEOS. However, the silicate layer does influence the interaction between micelles as observed from lifetime fluorescence analysis. The presence of a silicate layer hindered the exchange of pyrene from micelle to micelle, but was not dependent on the amount of silicate present. Even a small amount of TEOS was able to prevent the exchange of pyrene indicating less interaction between the micelle cores.

Chapter 4: Nanoemulsions and their Application as Nanoreactors

The silicate hybrid micelle template was demonstrated to be adaptive and flexible. Studies on more complex O/W and W/O nanoemulsions used as porosity templates and nanoreactors were conducted. The intrinsic dynamics and flexibility of these systems have proven to be a drawback for their broader use in material synthesis. This study was aimed at exploring the ability to reduce these intrinsic properties by introducing a liquid-to-solid switch replacing the internal liquid oil phase with a solid wax phase. The present chapter describes how the structure and stability of nanoemulsions are influenced by the chemical composition and synthesis conditions.

4.1 Experimental Methods

Span80 and Tween80 were the surfactants used to synthesize oil in water nanoemulsions. Span80 (sorbitane monooleate) has an HLB value of 4.3 while Tween80 (an ethoxy sorbitane monooleate ester) has an HLB value of 15. Both contain a similar structure with the same backbone, which allows these two surfactants to mix easily so that the HLB of the mixture can be controlled, according to Equation 4.1.[10]

$$HLB_T = HLB_{Span80} \text{ x } wt\%Span80 + HLB_{Tween80} \text{ x } wt\%Tween80 \quad (4.1)$$

where HLB_T is the HLB of the final mixture of surfactants, wt%Span80 and wt%Tween80 are the mass percent of Span80 and Tween80 respectively, and HLB_{Span80} and $HLB_{Tween80}$ are the HLBs of Span80 and Tween80, respectively.

Wax/Oil in water nanoemulsions were synthesized using the PIC method.[7] For a typical 100 g synthesis, approximately 2.25 g of Span80, 4.77 g of Tween80, and the oil

phase were weighed out into a round bottom flask. The oil phase was a mixture of paraffin oil and paraffin wax ($C_{20}H_{42}$) with approximately 6 g of wax and 14 g of oil. The surfactants and oil phase were submersed in a water bath heated to 70 ºC (in order to melt the wax) and mixed under gentle magnetic stirring (between 60 and 200 rpm). Once mixed, 73.0 g of water heated to 70 ºC is added drop-by-drop at a rate of approximately 2 mL/min. Once all the water was added, the solution was removed from the water bath and left to stir at room temperature until cooled. DLS was used to determine the hydrodynamic diameter of the nanoemulsions.

Water-in-oil nanoemulsions were prepared using the PIC method using the work done by Hong et al. as a basis.[78] For a typical 100 g synthesis approximately 69.18 g of paraffin oil, 1.55 g of Brij35, and 6.21 g of Span80 were weighed in a beaker. The surfactants and paraffin oil were heated to 70 ºC and mixed under gentle magnetic stirring (between 60 and 200 rpm). In a round bottom flask, 23.06 g of deionized water was weighed out and submersed in a water bath at 70 ºC under gentle magnetic stirring (between 60 and 200 rpm). The oil and surfactants were added to the water drop-by-drop at a rate of approximately 2 mL/min. Once all of the oil phase was added, the solution was taken out of the water bath and left to stir until it cooled. Surfactant composition and synthesis temperature were varied for other samples. DLS was used to determine the hydrodynamic diameter of the nanoemulsions.

Prussian blue analogues (PBAs) were synthesized by using the water phase in the W/O nanoemulsions as reactors. The same procedure was used as for the typical W/O nanoemulsion synthesis with 34.59 g of paraffin oil, 0.78 g of Brij35, 3.11 g of Span80, and 11.53 g of deionized water. For these nanoemulsions, either metallocyanate or metal

salt was dissolved in the water before addition of the oil phase. The final product was obtained by mixing the two different nanoemulsions.

Eight separate nanoemulsions with two containing metallocyanate precursors, $K_3Fe(CN)_6$ (0.30 g) and $K_3Co(CN)_6$ (0.30 g), and six containing a different metal salt, $FeCl_3 \cdot 6H_2O$ (0.41 g), $Ni(NO_3)_2 \cdot 6H_2O$ (0.44 g), $FeCl_2 \cdot 4H_2O$ (0.30 g), $Sm(NO_3)_3 \cdot 6H_2O$ (0.67 g), $CuCl_2 \cdot 2H_2O$ (0.26 g), and $Co(NO_3)_2 \cdot 6H_2O$ (0.44 g). To synthesize the PBAs, 5.00 g of each nanoemulsion containing cyanate precursor was mixed with 5.00 g of each of the nanomemulsions containing the metal salts producing twelve samples. We did not observe a very fast reaction, as usually observed when mixing aqueous solutions. The mixture was allowed to react overnight. The resulting mixture was washed with acetone and centrifuged at 5000 rpm to extract the solid PBA-MSU particles.

4.2 Droplet Size Control of Wax/Oil in Water Nanoemulsions

A brief test was done on the wax nanoemulsions in order to check whether or not droplet sizes could be controlled with a solid dispersed phase. Different ratios of paraffin wax to paraffin oil were used in this experiment to study the effect of the amount of wax on droplet size. Previous studies have been performed with different ratios of paraffin wax and paraffin oil in order to determine the melting temperature of the mixtures. Once the mixtures are heated up, one homogeneous phase is formed. Figure 20 displays the melting temperature for these mixtures as a function of the weight percent in paraffin wax.

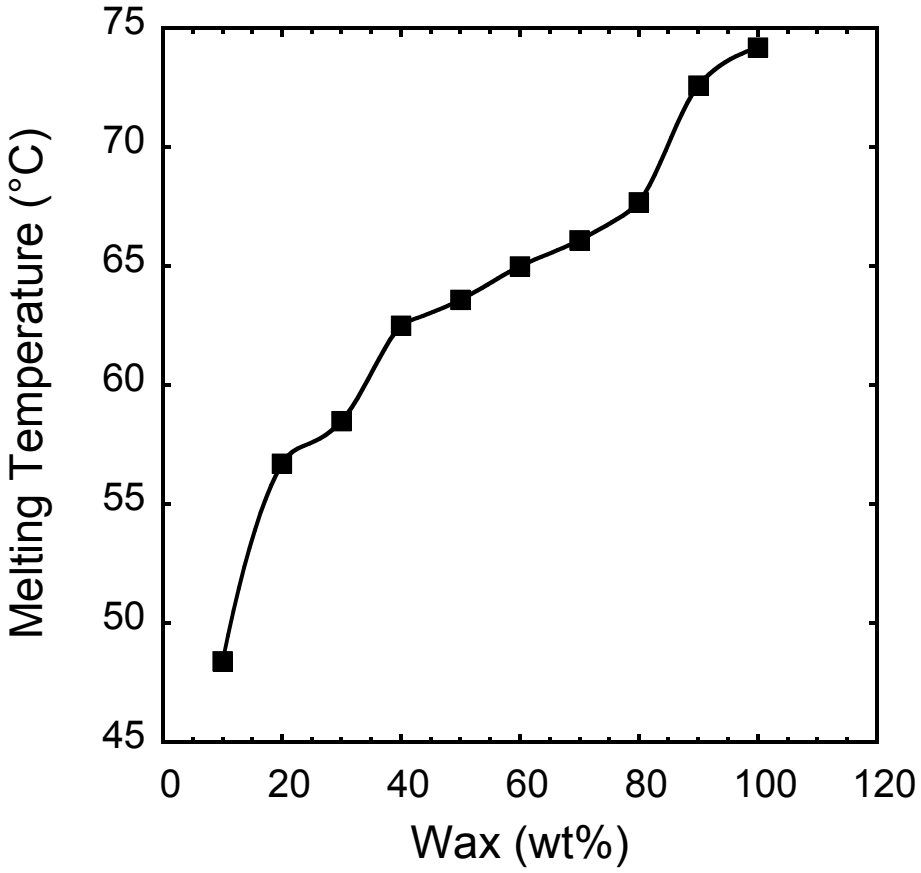

Figure 20: Onset Temperature of Different Paraffin Wax/Oil Mixtures

The percentages of wax by mass of paraffin used were 0%, 10%, 20%, and 30%. All samples were prepared at 70°C and were cooled with an ice bath in an attempt to freeze the oil droplets before they coalesced. The particles hydrodynamic diameters as a function of weight percent in wax that were measured by DLS are shown in Figure 21 with a visual of the nanoemulsion displayed in Figure 22. The DLS measurements of the wax/oil nanoemulsions (Figure 23) have an accuracy of ± 2 nm. It is quite evident that increasing the amount of wax increases the oil/wax droplet size especially from 20% wax to 30% wax.

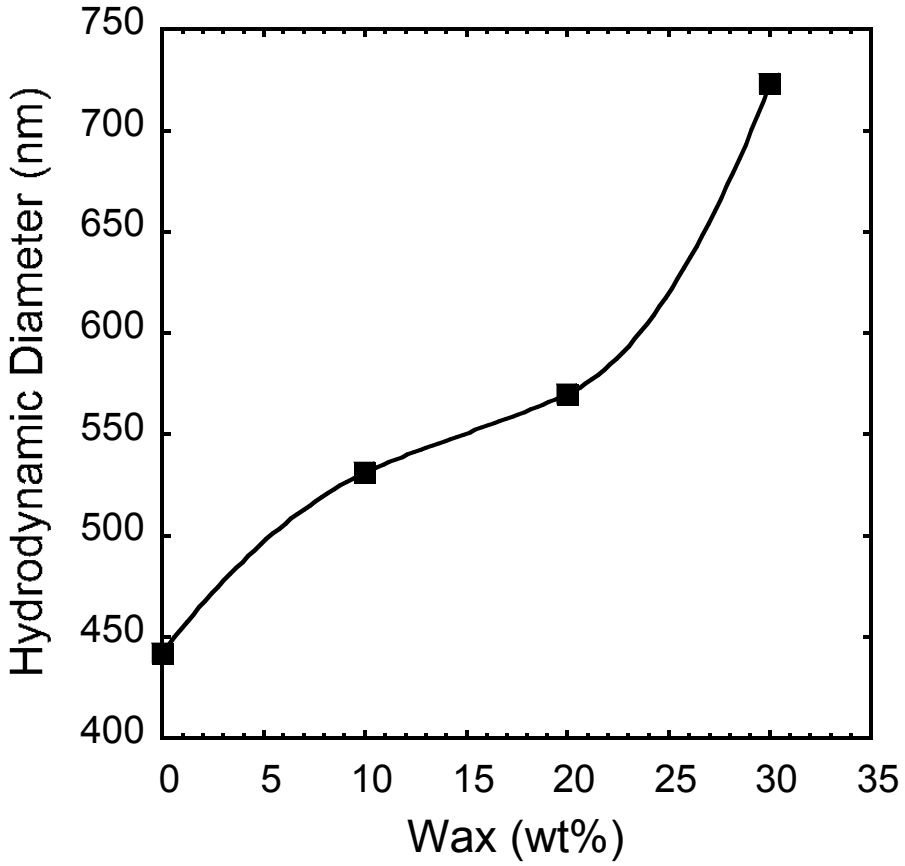

Figure 21: Hydrodynamic diameter of wax/oil nanoemulsions as function of weight percent in wax with ± 2 nm accuracy

Figure 22: Wax Nanoemulsion (30% Wax/Oil Ratio)

4.3 Preparation of Water in Oil Nanoemulsions Using the PIC Method

Water-in-oil nanoemulsions were prepared at different temperatures with surfactant mixtures having different HLB values to probe variations in the hydrodynamic diameter of the water droplets. The two synthesis temperatures studied were 70 ºC and

80 ºC and the two HLBs had values of 6.4 (1.30 g of Brij35 and 6.46 g of Span80) and 6.8 (1.54 g of Brij35 and 6.22 g of Span80). Table 1 displays the size (hydrodynamic diameter) of these 4 nanoemulsions. Although it is a very brief look into the w/o nanoemulsion system, it demonstrates the ability to adapt the water droplet size based on modification of HLB and synthesis temperature, as was previously demonstrated for the O/W nanoemulsions.

Table 1: Water Droplet Hydrodynamic Diameter of W/O Nanoemulsions

HLB	Size (nm) 70 ºC	Size (nm) 80 ºC
6.4	153	70
6.8	54	140

4.4 PBA-MSU Synthesized Using Water in Oil Nanoemulsions as Templates

A brief study was performed to determine if the water droplets in W/O nanoemulsions can be used as nanoreactors to synthesize PBA-MSU. Figure 23 shows the nanoemulsions with the metallocyanate ($K_3Co(CN)_6$) and metal salt ($FeCl_2 \cdot 4H_2O$), while Figure 24 displays the resulting mixture once the two are combined. The resulting mixture is later washed and centrifuged with acetone to obtain the PBA-MSU particles. The resulting powders formed from all combinations of metal salts and metal cyanates can be seen in Appendix C.

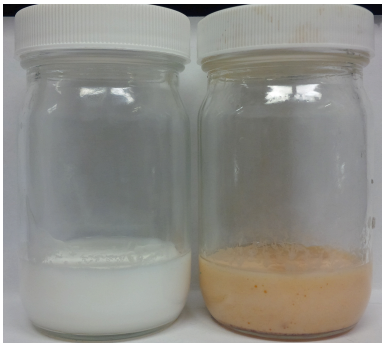

Figure 23: (Left): W/O Nanoemulsion containing $K_3Co(CN)_6$ (Right): W/O Nanoemulsion containing $FeCl_2 \cdot 4H_2O$

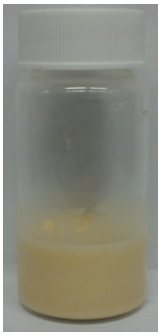

Figure 24: Mixture of $K_3Co(CN)_6$ and $FeCl_2 \cdot 4H_2O$ resulting in blue Fe(II)Co(III) PBA

The PBA-MSU particles were analyzed using FTIR to identify if a reaction occurred between the two precursors. The unreacted free CN^- ions show a stretch in the FTIR spectra at approximately 2080 cm^{-1}, whereas the reacted CN^- ions (in this case forming the $Fe_3Co(CN_6)_2$ complex) show a vibrational mode at 2180 cm^{-1}. Figure 25 shows the vibrational mode with a distinct peak indicating the reaction taking place between the two W/O nanoemulsions. Appendix C displays the FTIR spectra for the other eleven samples. With the exception of the samples combining $K_3Fe(CN)_6$ with $Co(NO_3)_2.6H_2O$ and $K_3Fe(CN)_6$ with $FeCl_2.4H_2O$, all other samples showed clear peaks at 2180 cm^{-1} indicating reaction of the cyanate ions with the metals.

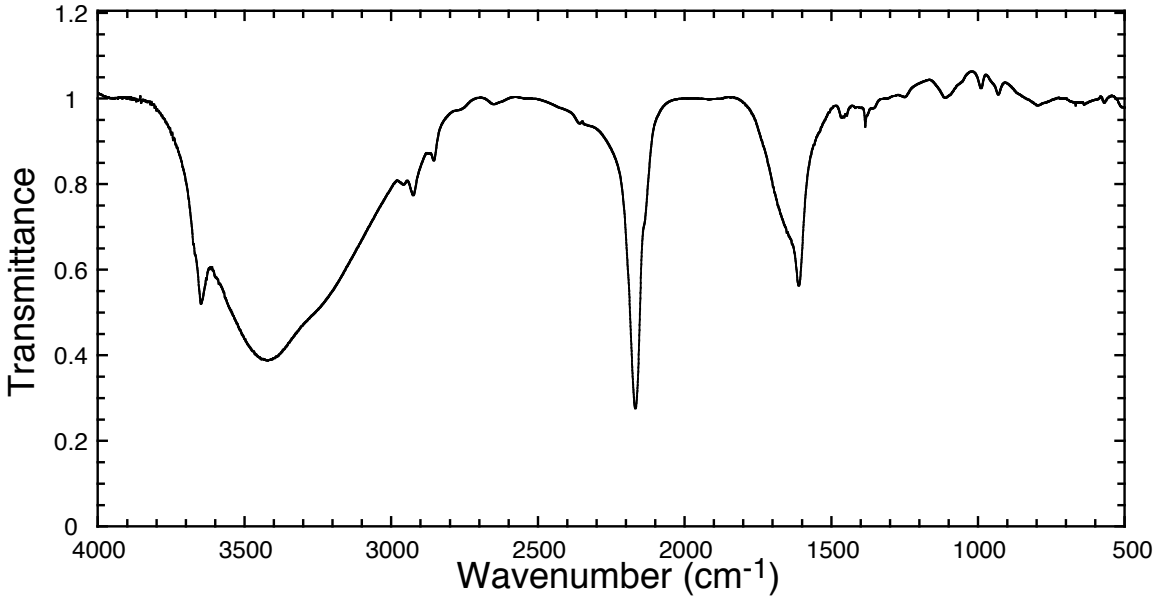

Figure 25: FTIR Spectrum of $Fe_3(Co(CN)_6)_2$ showing a distinct peak at approximately 2180 cm^{-1}

In addition, the samples producing $Co_3(Co(CN)_6)_2$ and $Ni_3(Co(CN)_6)_2$ were characterized using X-ray diffraction to deduce whether or not the diffraction peaks common to Prussian Blue Analogues were present. These figures can be seen in Appendix C (Figure C 14 and Figure C 15). Both of these samples showed four clear diffraction peaks, which are labeled with their respective miller indices in the figures.

4.5 The Nanoemulsion System and their Use as Templates

Nanoemulsions have been more commonly known to have a liquid dispersed phase. This work demonstrates the ability to synthesize nanoemulsions that have a solid dispersed phase by using a combination of wax and oil for the apolar phase. We show the ability to control the size of the dispersed phase by varying the percentage of wax used.

We also briefly investigate the use of a new w/o nanoemulsion system and the ability to tune the size of the water droplets. Based on synthesis temperature and HLB

alone, there is evidence that droplet size can be controlled. The previous works carried out in the group demonstrated that O/W nanoemulsions could be used for the synthesis of metal oxide nanoparticles within the water phase. However, the use of the confined oily phase required that the metal precursors had to be complexed with hydrophobic ligands to be inserted into the nanoemulsion. The present report demonstrates that the same chemistry could be conducted with aqueous nanoemulsions, which expands the domain of synthesis much further. With control of these droplet sizes, we can then synthesize nanoparticles having particular dimensions. Prussian blue analogues were shown to be synthesized using the water phase as the reactors for metal salts and metal cyanates to react and form PBA-MSU. This was verified by characterization through FTIR and XRD. No additional analysis was conducted due to a lack of time.

Chapter 5: Silicate Hybrid Micelles Used for Synthesis of HPLC Beads

We demonstrated the adaptability and dynamic behaviour of soft matter systems. This study focused on the silica particles that could be synthesized using silicate hybrid micelles as templates. We show how the rate of silica condensation and nucleation and growth controlled by catalyst concentration and temperature can affect the final morphology of the silica particles. Previous studies done by Nakanishi demonstrated how to synthesize silica with a gyroid like structure. These structures proved to have an effective pore topology for HPLC.[79-81] Our silica powders displayed the same type of gyroid structures and were validated for their potential as HPLC column beads.

5.1 Experimental Methods

Silicate hybrid micelles provide a useful template that can produce mesoporous silica with a variety of properties. Once in solution, a silica reaction can be initiated using a catalyst and mesoporous silica is formed through nucleation and growth. A variety of surfactants were used as templates to prepare mesoporous silica (see Appendix B for other surfactants and compositions that have been tested). Tergitol 15-S-12 was one of the surfactants investigated due to previous knowledge regarding the behavior of this template. In a typical synthesis, 11.10 g of Tergitol 15-S-12 was dissolved in 150 mL of water (pH 2). After complete dissolution, 62.5 g of TEOS was added drop by drop under stirring at 500 rpm. The solution turned cloudy immediately after the addition of TEOS. TEOS was left to stir until it turned clear, indicating that it had been hydrolyzed. This solution was then split into 4 equal amounts. A second solution was prepared by dissolving 2.0 g of sodium alginate in 30 mL of water (pH 2). This solution was also

split into 4 equal amounts. The 4 solutions of silicate hybrid micelles were each poured into the solutions of sodium alginate and mixed until 4 homogenous solutions were obtained. These solutions were then reacted using sodium fluoride to initiate the silica condensation. A 1.0 M solution of sodium fluoride was prepared. From this solution, a different amount of sodium fluoride was placed in each of the four solutions prepared: 1.5 mL, 3.0 mL, 4.5 mL, and 6.0 mL. The solutions were then left at room temperature for 1.5 hours and then placed in the oven for drying at 90 ^{0}C overnight. Each sample was then sonicated in order to break the solid structure into a powder and was vacuum filtered using ethanol. All samples were calcined (see Appendix B for calcination profile). The synthesis can be performed at different temperatures by heating the samples before addition of sodium fluoride. These samples are referred to as HPLC_X_y_T where X is the type of surfactant, y is the percentage of sodium fluoride with respect to the number of moles of TEOS added, and T is the synthesis temperature.

5.2 Mesoporous Silica Prepared from Silicate Hybrid Micelle Templates

This study was an extension of the work done by Sean O'Neil (initial work) and was done in collaboration with Takuto Kwok and Susan Nguyen. Synthesis was performed at 20, 25, and 30 ^{0}C in order to study the influence of temperature on the structure of the silica particles, giving a total of 12 different samples. In order to observe the type of structure produced, SEM photos were taken. Figures 26 and 27 show the SEM photos of HPLC_Brij58_8_25 (overnight) and HPLC_Brij58_8_25 respectively. The overnight sample was left to age for one day before the catalyst was added to react

the silica. The overnight sample had a BET surface area of 671.2 m^2/g while the other sample had a BET surface area of 19.1 m^2/g.

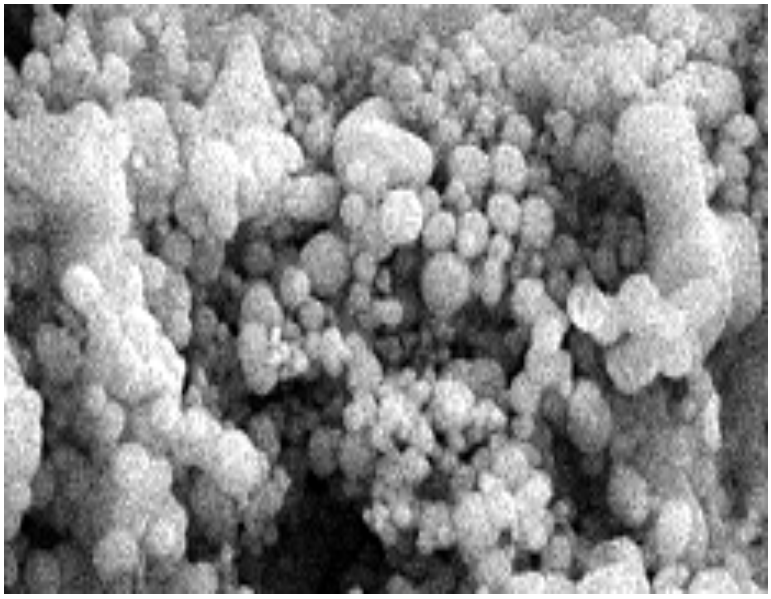

Figure 26: SEM of HPLC_Brij58_8_25 (overnight) showing low magnification of silica particles with high surface area

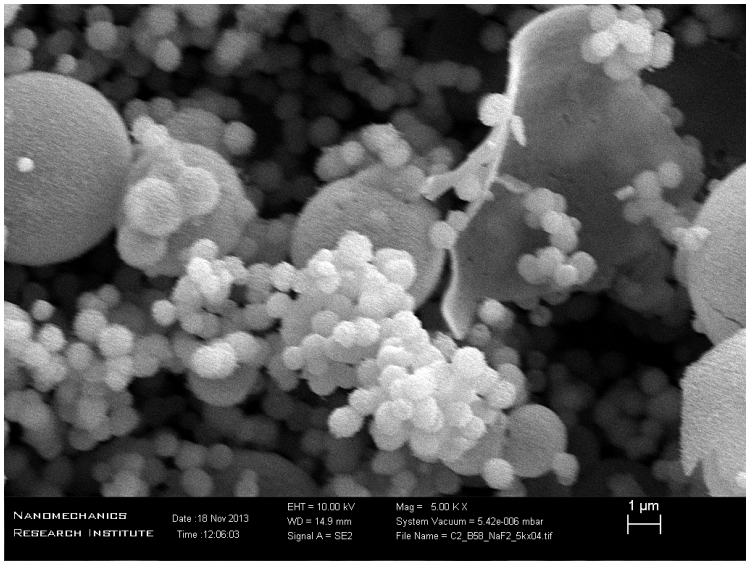

Figure 27: SEM of HPLC_Brij58_8_25 showing silica particles having a low surface area

Another surfactant used for this synthesis was Brij98. Figures 28 and 29 show the SEM pictures of HPLC_Brij98_2_25 and HPLC_Brij98_4_25. Their respective BET surface areas are 137.9 m^2/g and 6.0 m^2/g.

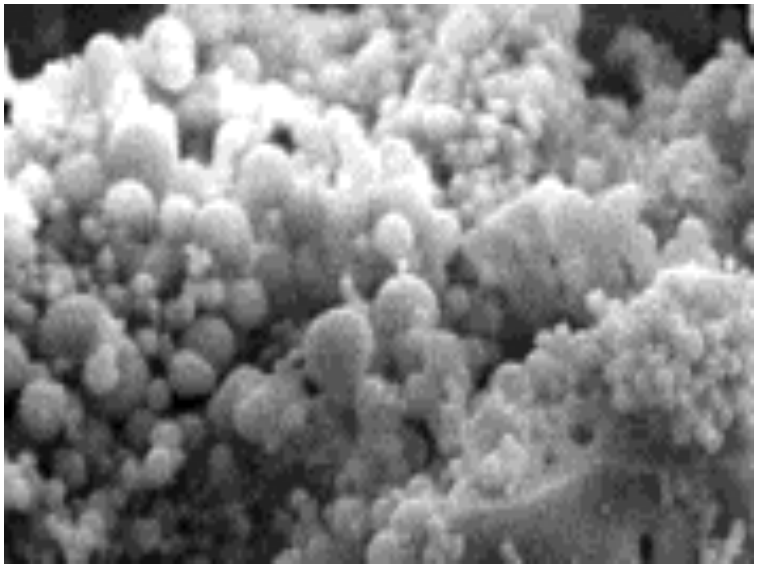

Figure 28: SEM of HPLC_Brij98_2_25 showing silica particles having a relatively high surface area

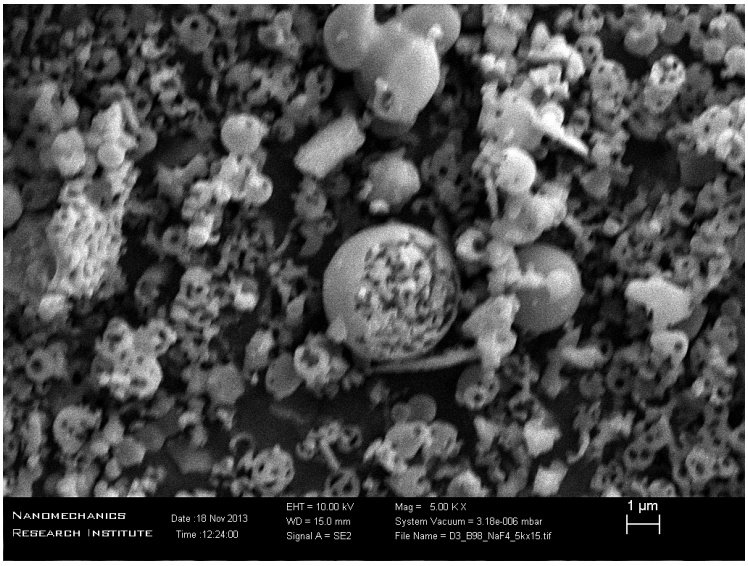

Figure 29: SEM of HPLC_Brij98_4_25 showing silica particles having low surface area

A third surfactant was used, Tergitol 15-S-12, which would ultimately produce the particles with the highest potential for HPLC. Figure 30 and 31 display the SEM photos for HPLC_T15-S-12_2_20 and HPLC_T15-S-12_2_20, which have respective surface areas of 70.5 m^2/g and 7.9 m^2/g.

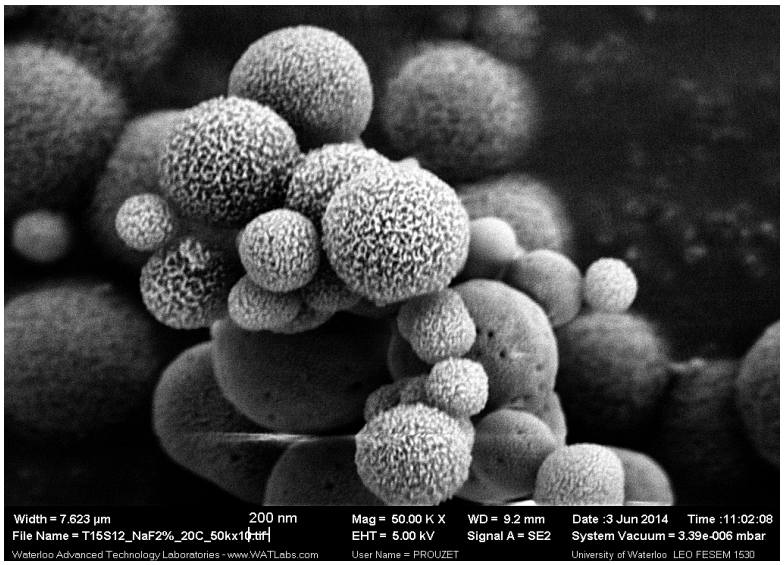

Figure 30: SEM of HPLC_T15-S-12_2_20 showing spherical particles

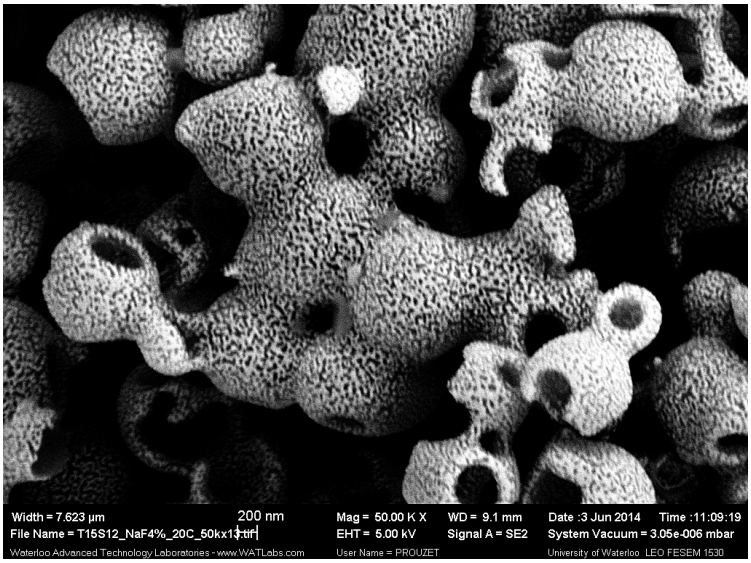

Figure 31: SEM of HPLC_T15-S-12_4_20 showing spherical particles with cavities

For samples synthesized at low temperatures with low sodium fluoride concentrations, conventional spherical particles with no observable pores and relatively high surface areas were obtained. Figure 32 shows the SEM photo of HPLC_T15-S-12_6_20 at the 200 nm scale. These silica particles showed porosity with an open structure. The open structure of these particles is due to the amount of space that the pores take up. This type

of structure has potential applications in HPLC columns for separation. Molecules of different sizes will travel through the gyroid surfaces and remain in the column for different amounts of time based on their size. Silica particles synthesized at 25 and 30 ^{0}C showed the presence of this type of structure, with only the homogeneity being different (HPLC_T15-S-12_6_20 showed the most homogenous gyroid structure).

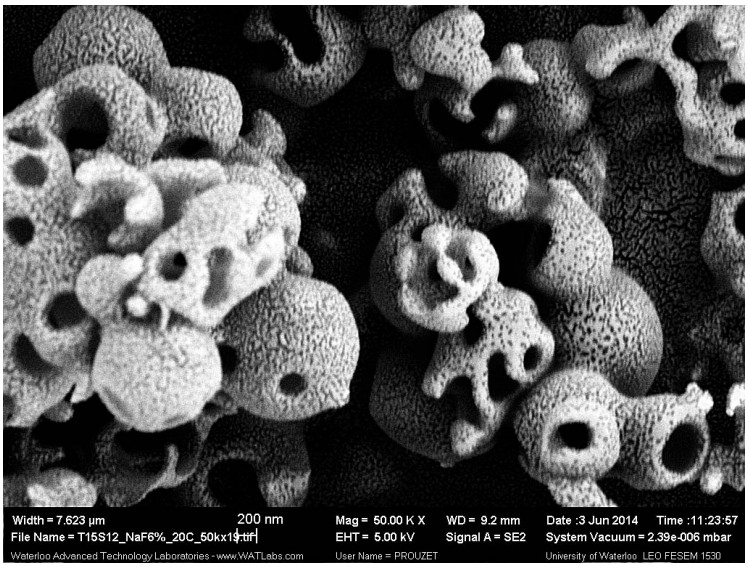

Figure 32: SEM of HPLC_T15-S-12_6_20 showing gyroid like structures

Additional SEM photos for other synthesis parameters are displayed in Appendix B. The general trends that were observed were that a faster reaction (i.e. more sodium fluoride or higher temperature) resulted in a more open structure with a lower BET surface area.

5.3 HPLC Column Preliminary Tests

The HPLC_T15-S-12_6_20 sample was grafted using trimethyl(octadecyl)silane. The resulting sample was sent to Belgium to be packed in a column. The column was

packed with 80:20 wt% hexane/isopropanol for 120 minutes at 650 bar. The column has a 2.1 mm inner diameter, 5 cm length, and 5 micron frits. The analyses were performed using an Agilent 1260 Series Liquid Chromatography apparatus (agilent Technologies) with a G1379B degasser, G1312B binary pump, G1329B autosampler, G1316B column oven, and G1315C DAD detector.

This column was tested first using three different mobile phases each at 25 , 40 and 50 ^{0}C in order to determine the pressure in the column as a function of the flow rate of these phases. The three mobile phases used were acetonitrile (ACN), methanol, and a water:ACN mixture containing a 9:1 ratio of water to ACN. All of these liquid phases showed a linear increase in pressure with increasing flow rate. At 25 ^{0}C, methanol increased from approximately 50 bar at 0.050 mL/min to 400 bar at 0.400 mL/min. At the same temperature, ACN had a pressure of 60 bar at 0.050 mL/min increasing to 510 bar at 0.400 mL/min. The mixture of water and ACN produced a pressure of 190 bar at 0.050 mL/min increasing to 520 bar at 0.150 mL/min. We observe that there is a drastic increase in pressure for the water and ACN mixture even at low flow rates because the viscosity of this liquid mixture is much higher than that of ACN or methanol. When the temperature was increased to 40 ^{0}C and 50 ^{0}C, there was a decrease in the pressure created by all three mobile phases. This is due to a decrease in the viscosity of the liquid. These trends can be found in Appendix B (Figure B 6 to Figure B 8).

A second test was performed where 4 compounds were placed in a mobile phase of a 40:60 ratio of ACN to water with a flow rate of 0.150 mL/min to be separated. The mixture contained 65.0 µg/mL of uracil, 64.9 µg/mL of toluene, 55.0 µg/mL of naphthalene, and 65.0 µg/mL of 2-fluorbiphenyl. We used a wavelength of 210 nm to

detect the presence of any compounds. Figure 33 displays the resulting separation of the 4 different compounds. The total process took approximately 10 minutes. We observe very sharp elution peaks demonstrating that the column is quite selective.

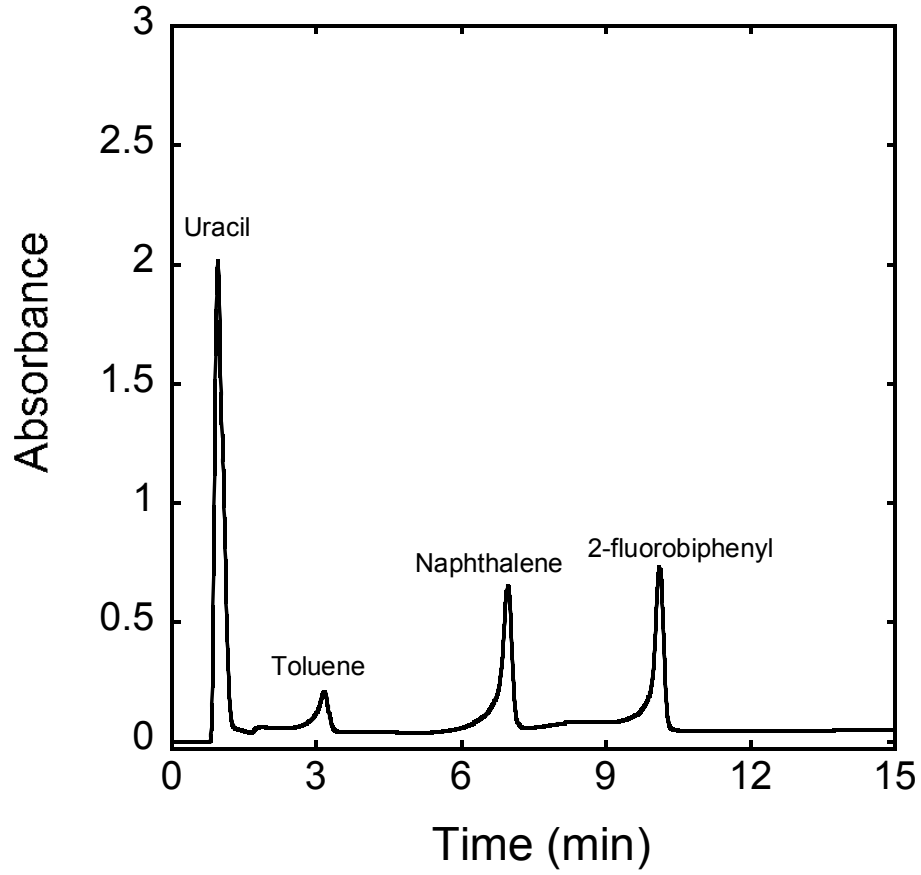

Figure 33: Chromatogram showing separation of uracil, toluene, naphthalene, and 2-fluorobiphenyl in 10 minutes using 40:60 ACN:water mobile phase.

5.4 Mesoporous Silica and its Application for HPLC

We demonstrated that the morphology of mesoporous silica synthesized from silicate hybrid micelle templates can be tuned based on the synthesis temperature and catalyst concentration. There are optimum kinetics that must exist for the gyroid like structures to be formed. The work done by Nakanishi led to the synthesis of similar gyroid like structures. However, the size of these structures was on the order of microns

and they were monolithic.[79-80] Our structures are on the order of nanometers and are powders containing silica beads. Unlike Nakanishi, we employed sodium fluoride as a condensation catalyst. The results showed that the faster the reaction was (more catalyst added), the smaller our particles would be (and surface area was significantly decreased). Having the rate of condensation increased by increasing the catalyst concentration increases the rate of nucleation and prevents the particles from growing. During the condensation process, it is also believed that the surfactant template is expelled from the system. This is believed to be the reason for the formation of the open structure, where the voids are formed due to the presence of surfactant during the expulsion process. Removal of the surfactant later leaves only the open structure.

Once synthesized, these gyroid structures can be grafted with trimethyl(octadecyl)silane, which is a common compound for HPLC. Once packed into an HPLC column, we show that these silica particles can be used for chromatography with great success. Separation of 4 benzophenones was successfully performed in a short period of time with good selectivity, showing a great potential for these silica particles in this application. The drawbacks of the monolithic structures synthesized by Nakanishi are the lack of homogeneity in sub-micron structures that would greatly improve the HPLC column effectiveness.[81] We synthesized particles that have nanometer scale structures, while still retaining the properties of micrometer monolithic structures used for HPLC. With improved homogeneity, these particles could prove to be a leader in HPLC columns.

Chapter 6: Conclusion and Future Work

This work has examined a number of different surfactants that can be used as templates for silicate hybrid micelles. Previous results have shown that the size of silicate hybrid micelles is a function of temperature. We demonstrate that the size of the silicate hybrid micelles varies in the same way that the surfactant micelles behave over the same temperature range. It was initially believed that micelles increase in size with increasing temperature due to the surfactant molecules becoming more hydrophobic. This behavior is not observed for all types of surfactant due to the differences in their structures. Some surfactant micelles do not vary significantly in size as a function of temperature. However, the behavior that is observed for the surfactant micelles alone is also observed for the respective silicate hybrid micelles, indicating that the behavior is retained even with a silicate layer added.

We also investigate the impact of the silicate layer on the formation and interaction of micelles for one surfactant by using fluorescence spectroscopy. The presence of silicate at all concentrations had no impact on the critical micelle concentration. However, silicate hybrid micelles have an inorganic shell that prevents them from interacting with each other. This was not the case with pure micelles, which showed interaction with each other in solution.

We also briefly examined nanoemulsions and their potential as nanoreactors to synthesize silica nanoparticles of a particular size. We used metals salts and metal cyanates to synthesize Prussian blue analogues. We showed that nanoemulsion droplet sizes can be varied based on synthesis parameters and that w/o nanoemulsions in particular can be used to synthesize PBA-MSU.

We applied the silicate hybrid micelle template to synthesize mesoporous silica. With a particular synthesis temperature and catalyst concentration, we were able to obtain open silica structures with gyroid shapes. This morphology has a lot of potential in HPLC applications to improve upon the speed and efficiency in separating compounds. Preliminary tests were performed on the separation of 4 compounds with very good selectivity observed in a reasonably quick elution time.

Future work for the silicate hybrid micelles would include extending the number of surfactants that have been used as templates. It is also necessary to finish fluorescence studies on more than one of the surfactants used to synthesize silicate hybrid micelles to determine how silicate can affect the formation and interaction of micelles if the surfactant has a different structure.

The nanoemulsions and PBA-MSU require further experimentation to better understand the systems. Knowledge regarding the tunability of the nanoemulsions and the parameters that influence droplet size are required. For PBA-MSU, further characterization needs to be done regarding the final structures in order to deduce whether or not the template and particle dimensions coincide with each other. XRD should also be performed on the remaining samples to confirm the synthesis of PBAs.

For the mesoporous silica with open gyroid structure, the synthesis parameters must be investigated further to improve upon the homogeneity of the particles formed. Currently, gyroid structures are evident, but there are a lot of solid silica spheres that can be seen as impurities for HPLC applications. HPLC tests using a packed column with the silica should also be tested further to determine the optimal parameters to be used for separation.

References

1. Burkett, S. L.; Sims, S. D.; Mann, S., Synthesis of hybrid inorganic-organic mesoporous silica by co-condensation of siloxane and organosiloxane precursors. *Chem. Comm.* **1996,** (11), 1367-1368.
2. Sanchez, C.; Rozes, L.; Ribot, F.; Laberty-Robert, C.; Grosso, D.; Sassoye, C.; Boissiere, C.; Nicole, L., "Chimie douce": A land of opportunities for the designed construction of functional inorganic and hybrid organic-inorganic nanomaterials. *Comptes Rendus Chimie* **2010,** *13* (1-2), 3-39.
3. Destribats, M.; Faure, B.; Birot, M.; Babot, O.; Schmitt, V.; Backov, R., Tailored Silica Macrocellular Foams: Combining Limited Coalescence-Based Pickering Emulsion and Sol-Gel Process. *Advanced Functional Materials* **2012,** *22* (12), 2642-2654.
4. Prouzet, E.; Ravaine, S.; Sanchez, C.; Backov, R., Bio-inspired synthetic pathways and beyond: integrative chemistry. *New Journal of Chemistry* **2008,** *32* (8), 1284.
5. Hessien, M.; Singh, N.; Kim, C.; Prouzet, E., Stability and Tunability of O/W Nanoemulsions Prepared by Phase Inversion Composition. *Langmuir* **2011**.
6. Liu, W.; Sun, D.; Li, C.; Liu, Q.; Xu, J., Formation and stability of paraffin oil-in-water nano-emulsions prepared by the emulsion inversion point method. *J. Colloid Interface Sci.* **2006,** *303* (2), 557-63.
7. Li, C.; Mei, Z.; Liu, Q.; Wang, J.; Xu, J.; Sun, D., Formation and properties of paraffin wax submicron emulsions prepared by the emulsion inversion point method. *Colloids Surf. A: Physicochem. Eng. Aspects* **2010,** *356* (1-3), 71-77.

8. Boissiere, C. v. d. L., A; Mansourie, Abdeslam; Larbot, A; Prouzet, E., A double step synthesis of mesoporous micrometric spherical MSU-X silica particles. *Chem. Comm.* **1999**, 2047-2048.

9. Prouzet, E.; Pinnavaia, T. J., Assembly of mesoporous molecular sieves containing wormhole motifs by a nonionic surfactant pathway: Control of pore size by synthesis temperature. *Angewandte Chemie-International Edition* **1997,** *36* (5), 516-518.

10. Hessien, M. Metal Oxide-Hierarchical Porous Silica Nanocomposites Prepared by Nanoemulsion Templating and Integrative Synthesis. University of Waterloo, 2012.

11. Melghit, K., Soft Chemistry Routes to New Nanosize Materials. *J. Sci.* **2007,** *12* (2), 87-100.

12. Hench, L. L.; West, J. K., THE SOL-GEL PROCESS. *Chemical Reviews* **1990,** *90* (1), 33-72.

13. Brinker, C. J., Hydrolysis and condensation of silicates: Effects on structure. *Journal of Non-Crystalline Solids* **1988,** *100* (1–3), 31-50.

14. *Colloidal Silica Fundamentals and Applications*. Taylor and Francis Group: 2006.

15. Brinker, C. J. S., George W., *Sol-Gel Science: The Physics and Chemistry of Sol-Gel Processing*. Academic Press Limited: 1990.

16. Niederberger, M. P., Nicola, *Metal Oxide Nanoparticles in Organic Solvents*. Springer-Verlag London Limited: 2009; p 11.

17. Livage, J.; Sanchez, C., SOL-GEL CHEMISTRY. *Journal of Non-Crystalline Solids* **1992,** *145* (1-3), 11-19.

18. Son, J. H.; Park, H. Y.; Kang, D. P.; Bae, D. S., Synthesis and characterization of Ag/Pd doped SiO2 nanoparticles by a reverse micelle and sol–gel processing. *Colloids Surf. A: Physicochem. Eng. Aspects* **2008,** *313-314*, 105-107.

19. Martines, M. A. U.; Yeong, E.; Larbot, A.; Prouzet, E., Temperature dependence in the synthesis of hexagonal MSU-3 type mesoporous silica synthesized with Pluronic P123 block copolymer. *Microporous and Mesoporous Materials* **2004,** *74* (1-3), 213-220.

20. Li, D.; Li, H.; Fu, Y.; Zhang, J.-L.; Li, W.; Han, Y.-C.; Wang, L., Critical micelle concentrations of cetyltrimethylammonium chloride and their influence on the periodic structure of mesoporous silica. *Colloid Journal* **2008,** *70* (6), 747-752.

21. Mackenzie, J. D., APPLICATIONS OF THE SOL-GEL PROCESS. *Journal of Non-Crystalline Solids* **1988,** *100* (1-3), 162-168.

22. Maali, A.; Mosavian, M. T. H., Preparation and Application of Nanoemulsions in the Last Decade (2000–2010). *J. Dispersion Sci. Tech.* **2013,** *34* (1), 92-105.

23. McClements, D. J., Nanoemulsions versus microemulsions: terminology, differences, and similarities. *Soft Matter* **2012,** *8* (6), 1719.

24. Rao, J. J.; McClements, D. J., Lemon oil solubilization in mixed surfactant solutions: Rationalizing microemulsion & nanoemulsion formation. *Food Hydrocolloids* **2012,** *26* (1), 268-276.

25. Anton, N.; Benoit, J. P.; Saulnier, P., Design and production of nanoparticles formulated from nano-emulsion templates-a review. *J Control Release* **2008,** *128* (3), 185-99.

26. Beattie, J. K.; Djerdjev, A. M., The pristine oil/water interface: surfactant-free hydroxide-charged emulsions. *Angew Chem Int Ed Engl* **2004,** *43* (27), 3568-71.

27. Mason, T. G.; Wilking, J. N.; Meleson, K.; Chang, C. B.; Graves, S. M., Nanoemulsions: formation, structure, and physical properties. *Journal of Physics: Condensed Matter* **2006,** *18* (41), R635-R666.

28. Solè, I.; Maestro, A.; Pey, C. M.; González, C.; Solans, C.; Gutiérrez, J. M., Nano-emulsions preparation by low energy methods in an ionic surfactant system. *Colloids Surf. A: Physicochem. Eng. Aspects* **2006,** *288* (1-3), 138-143.

29. Solans, C.; Solé, I., Nano-emulsions: Formation by low-energy methods. *Current Opinion in Colloid & Interface Science* **2012,** *17* (5), 246-254.

30. Mira, I.; Zambrano, N.; Tyrode, E.; Marquez, L.; Pena, A. A.; Pizzino, A.; Salager, J. L., Emulsion catastrophic inversion from abnormal to normal morphology. 2. Effect of the stirring intensity on the dynamic inversion frontier. *Industrial & Engineering Chemistry Research* **2003,** *42* (1), 57-61.

31. Tyrode, E.; Mira, I.; Zambrano, N.; Marquez, L.; Rondon-Gonzalez, M.; Salager, J. L., Emulsion catastrophic inversion from abnormal to normal morphology. 3. Conditions for triggering the dynamic inversion and application to industrial processes. *Industrial & Engineering Chemistry Research* **2003,** *42* (19), 4311-4318.

32. Zambrano, N.; Tyrode, E.; Mira, I.; Marquez, L.; Rodriguez, M. P.; Salager, J. L., Emulsion catastrophic inversion from abnormal to normal morphology. 1. Effect of the water-to-oil ratio rate of change on the dynamic inversion frontier. *Industrial & Engineering Chemistry Research* **2003,** *42* (1), 50-56.

33. Yu, L.; Li, C.; Xu, J.; Hao, J.; Sun, D., Highly stable concentrated nanoemulsions by the phase inversion composition method at elevated temperature. *Langmuir* **2012,** *28* (41), 14547-52.

34. Maestro, A.; Sole, I.; Gonzalez, C.; Solans, C.; Gutierrez, J. M., Influence of the phase behavior on the properties of ionic nanoemulsions prepared by the phase inversion composition method. *J. Colloid Interface Sci.* **2008,** *327* (2), 433-9.

35. Salager, J. L.; Forgiarini, A.; Marquez, L.; Pena, A.; Pizzino, A.; Rodriguez, M. P.; Rondon-Gonzalez, M., Using emulsion inversion in industrial processes. *Adv Colloid Interface Sci* **2004,** *108-109*, 259-72.

36. Fernandez, P.; André, V.; Rieger, J.; Kühnle, A., Nano-emulsion formation by emulsion phase inversion. *Colloids Surf. A: Physicochem. Eng. Aspects* **2004,** *251* (1-3), 53-58.

37. Solans, C.; Izquierdo, P.; Nolla, J.; Azemar, N.; Garciacelma, M., Nano-emulsions. *Current Opinion in Colloid & Interface Science* **2005,** *10* (3-4), 102-110.

38. Ostertag, F.; Weiss, J.; McClements, D. J., Low-energy formation of edible nanoemulsions: factors influencing droplet size produced by emulsion phase inversion. *J. Colloid Interface Sci.* **2012,** *388* (1), 95-102.

39. Wang, L.; Li, X.; Zhang, G.; Dong, J.; Eastoe, J., Oil-in-water nanoemulsions for pesticide formulations. *J. Colloid Interface Sci.* **2007,** *314* (1), 230-5.

40. Izquierdo, P.; Feng, J.; Esquena, J.; Tadros, T. F.; Dederen, J. C.; Garcia, M. J.; Azemar, N.; Solans, C., The influence of surfactant mixing ratio on nano-

emulsion formation by the pit method. *J. Colloid Interface Sci.* **2005,** *285* (1), 388-94.

41. Forgiarini, A.; Esquena, J.; González, C.; Solans, C., The Relation Between Phase Behavior and Formation of Narrow Size Distribution W/O Emulsions. *J. Dispersion Sci. Tech.* **2002,** *23* (1-3), 209-217.

42. Forgiarini, A. E., J.; Gonzalez, C.; Solans, C., Formation and stability of nano-emulsions in mixed noionic surfactant systems. *Prog. Colloid Sci.* **2001,** *118*, 184-189.

43. Giermanska, J. T., Florence; Backov, Renal; Schmitt, Veronique, Gelling of Oil-in-Water Emulsions Comprising Crystallized Droplets. *Langmuir* **2007,** *23*, 4792-4799.

44. Vigil, D. *The Jamming Transition in Granular Materials*; University of Illinois Urbana-Champaign: 2008.

45. Destribats, M.; Schmitt, V.; Backov, R., Thermostimulable wax@SiO2 core-shell particles. *Langmuir* **2010,** *26* (3), 1734-42.

46. Eder, F.; Huesing, N., Mesoporous silica layers with controllable porosity and pore size. *Applied Surface Science* **2009,** *256* (3), S18-S21.

47. Beck, J. S.; Vartuli, J. C.; Kennedy, G. J.; Kresge, C. T.; Roth, W. J.; Schramm, S. E., MOLECULAR OR SUPRAMOLECULAR TEMPLATING - DEFINING THE ROLE OF SURFACTANT CHEMISTRY IN THE FORMATION OF MICROPOROUS AND MESOPOROUS MOLECULAR-SIEVES. *Chemistry of Materials* **1994,** *6* (10), 1816-1821.

48. Cheng, C. F.; Luan, Z. H.; Klinowski, J., THE ROLE OF SURFACTANT MICELLES IN THE SYNTHESIS OF THE MESOPOROUS MOLECULAR-SIEVE MCM-41. *Langmuir* **1995,** *11* (7), 2815-2819.

49. Kim, J. M.; Han, Y. J.; Chmelka, B. F.; Stucky, G. D., One-step synthesis of ordered mesocomposites with non-ionic amphiphilic block copolymers: implications of isoelectric point, hydrolysis rate and fluoride. *Chem. Comm.* **2000,** (24), 2437-2438.

50. Zhang, Y.; Pu, M.; Wu, D.; Sun, Y. H.; Peng, S. Y., The creation of mesopore in silica gel by nonionic surfactant. *Acta Chimica Sinica* **2001,** *59* (12), 2148-2151.

51. Hoffmann, F.; Cornelius, M.; Morell, J.; Froba, M., Silica-based mesoporous organic-inorganic hybrid materials. *Angew Chem Int Ed Engl* **2006,** *45* (20), 3216-51.

52. Liu, J.; Yang, Q.; Zhao, X. S.; Zhang, L., Pore size control of mesoporous silicas from mixtures of sodium silicate and TEOS. *Microporous and Mesoporous Materials* **2007,** *106* (1-3), 62-67.

53. Beck, J. S.; Vartuli, J. C.; Roth, W. J.; Leonowicz, M. E.; Kresge, C. T.; Schmitt, K. D.; Chu, C. T. W.; Olson, D. H.; Sheppard, E. W., A new family of mesoporous molecular sieves prepared with liquid crystal templates. *J. Am. Chem. Soc.* **1992,** *114* (27), 10834-10843.

54. Bagshaw, S. A. P., Eric; Pinnavaia, Thomas J., Templating of Mesoporous Molecular Sieves by Nonionic Polyethylene Oxide Surfactants. *American Association for the Advancement of Science* **1995,** *269* (5228), 1242-1244.

55. Prouzet, E.; Cot, F.; Boissière, C.; Kooyman, P. J.; Larbot, A., Nanometric hollow spheres made of MSU-X-type mesoporous silica. *Journal of Materials Chemistry* **2002,** *12* (5), 1553-1556.

56. Prouzet, É.; Boissière, C., A review on the synthesis, structure and applications in separation processes of mesoporous MSU-X silica obtained with the two-step process. *Comptes Rendus Chimie* **2005,** *8* (3-4), 579-596.

57. de Zarate, D. O. B., F; Zschiedrich, H; Kooyman, P. J.; Trens, P.; Iapichella, J.; Duran, R; Guillem, C.; Prouzet, E., Micromesoporous Monolithic Al-MSU with a Widely Variable Content of Aluminum Leading to Tunable Acidity. *Chem. Mater.* **2008,** *20*, 1410-1420.

58. Attard, G. S.; Glyde, J. C.; Goltner, C. G., LIQUID-CRYSTALLINE PHASES AS TEMPLATES FOR THE SYNTHESIS OF MESOPOROUS SILICA. *Nature* **1995,** *378* (6555), 366-368.

59. Hessien, M.; Leone, P.; Suchaud, M.; LeBeau, B.; Nouali, H.; Guari, Y.; Prouzet, E., Nanocrystalline iron oxide synthesised within Hierarchical Porous Silica prepared by nanoemulsion templating. *Chem Commun (Camb)* **2012,** *48* (80), 10022-4.

60. Yang, Z.; Lu, Y.; Yang, Z., Mesoporous materials: tunable structure, morphology and composition. *Chem. Comm.* **2009,** (17), 2270-2277.

61. Ravetti-Duran, R.; Blin, J.-L.; Stébé, M.-J.; Castel, C.; Pasc, A., Tuning the morphology and the structure of hierarchical meso–macroporous silica by dual templating with micelles and solid lipid nanoparticles (SLN). *Journal of Materials Chemistry* **2012,** *22* (40), 21540.

62. Stein, A.; Rudisill, S. G.; Petkovich, N. D., Perspective on the Influence of Interactions Between Hard and Soft Templates and Precursors on Morphology of Hierarchically Structured Porous Materials. *Chemistry of Materials* **2014,** *26* (1), 259-276.

63. Szczech, J. R.; Lukowski, M. A.; Jin, S., Synthesis of mesoporous Si1-xGexO2 (0.10 <= x <= 0.31) using a nonionic block copolymer template. *Journal of Materials Chemistry* **2010,** *20* (38), 8389-8393.

64. Zhang, H. F.; Cooper, A. I., Synthesis and applications of emulsion-templated porous materials. *Soft Matter* **2005,** *1* (2), 107-113.

65. Wang, C.; Chen, D.; Jiao, X., Lyotropic liquid crystal directed synthesis of nanostructured materials. *Science and Technology of Advanced Materials* **2009,** *10* (2).

66. Wainwright, S. G.; Parlett, C. M. A.; Blackley, R. A.; Zhou, W.; Lee, A. F.; Wilson, K.; Bruce, D. W., True liquid crystal templating of SBA-15 with reduced microporosity. *Microporous and Mesoporous Materials* **2013,** *172*, 112-117.

67. Zhang, J.; Yu, M.; Yuan, P.; Wang, H.; Qian, K.; Tan, L.; Wang, Y.; Yu, C., Tuning cooperative vesicle templating and liquid crystal templating simply by varying silica source. *Journal of Materials Research* **2010,** *25* (4), 648-657.

68. Kim, A.; Black, R.; Hyun, Y. J.; Nazar, L. F.; Prouzet, E., Synthesis of monolithic meso-macroporous silica and carbon with tunable pore size. *Chem. Comm.* **2012,** *48* (36), 4335-4337.

69. Albayrak, C.; Soylu, A. M.; Dag, O., Lyotropic liquid-crystalline mesophases of Zn(H2O)(6) (NO3)(2)-C12EO10-CTAB-H2O and Zn(H2O)(6) (NO3)(2)-C12EO10-SDS-H2O systems. *Langmuir* **2008,** *24* (19), 10592-10595.

70. Surendran, G.; Ksar, F.; Ramos, L.; Keita, B.; Nadjo, L.; Prouzet, E.; Beaunier, P.; Dieudonne, P.; Audonnet, F.; Remita, H., Palladium nanoballs synthesized in hexagonal mesophases. *Journal of Physical Chemistry C* **2008,** *112* (29), 10740-10744.

71. Lehoux, A.; Ramos, L.; Beaunier, P.; Uribe, D. B.; Dieudonne, P.; Audonnet, F.; Etcheberry, A.; Jose-Yacaman, M.; Remita, H., Tuning the Porosity of Bimetallic Nanostructures by a Soft Templating Approach. *Advanced Functional Materials* **2012,** *22* (23), 4900-4908.

72. Boissiere, C.; Larbot, A.; Bourgaux, C.; Prouzet, E.; Bunton, C. A., A study of the assembly mechanism of the mesoporous MSU-X silica two-step synthesis. *Chemistry of Materials* **2001,** *13* (10), 3580-3586.

73. Gong, Y. J.; Wu, D.; Sun, Y. H.; Zhang, Z. D.; Zhu, H. G.; Zhao, D. Y., Double-mesopore V-MSU-X silica and its pure siliceous derivative prepared by one synthesis system. *Chinese Chemical Letters* **2001,** *12* (8), 747-750.

74. Sing, K. S. W., Physisorption of Nitrogen by Porous Materials. *Journal of Porous Materials* **1995,** *2*, 5-8.

75. Prouzet, E.; Boissière, C.; Kim, S. S.; Pinnavaia, T. J., Roughness of mesoporous silica surfaces deduced from adsorption measurements. *Microporous and Mesoporous Materials* **2009,** *119* (1-3), 9-17.

76. Butt, H.-J. G., Karlheins; Kappl, Michael, *Physics and Chemistry of Interfaces*. WILEY-VCH Verlag GmbH & Co.: 2003.

77. Keyes-Baig, C.; Duhamel, J.; Wettig, S., Characterization of the Behavior of a Pyrene Substituted Gemini Surfactant in Water by Fluorescence. *Langmuir* **2011,** *27* (7), 3361-3371.

78. Pan, H.; Yu, L.; Xu, J.; Sun, D., Preparation of highly stable concentrated W/O nanoemulsions by PIC Cross Mark method at elevated temperature. *Colloids and Surfaces a-Physicochemical and Engineering Aspects* **2014,** *447*, 97-102.

79. Nakanishi, K.; Soga, N., PHASE-SEPARATION IN SILICA SOL-GEL SYSTEM CONTAINING POLYACRYLIC-ACID .1. GEL FORMATION BEHAVIOR AND EFFECT OF SOLVENT COMPOSITION. *Journal of Non-Crystalline Solids* **1992,** *139* (1), 1-13.

80. Nakanishi, K.; Kobayashi, Y.; Amatani, T.; Hirao, K.; Kodaira, T., Spontaneous formation of hierarchical macro-mesoporous ethane-silica monolith. *Chemistry of Materials* **2004,** *16* (19), 3652-3658.

81. Nakanishi, K.; Tanaka, N., Sol-gel with phase separation. Hierarchically porous materials optimized for high-performance liquid chromatography separations. *Accounts of Chemical Research* **2007,** *40* (9), 863-873.

Appendix A: Silicate hybrid micelles

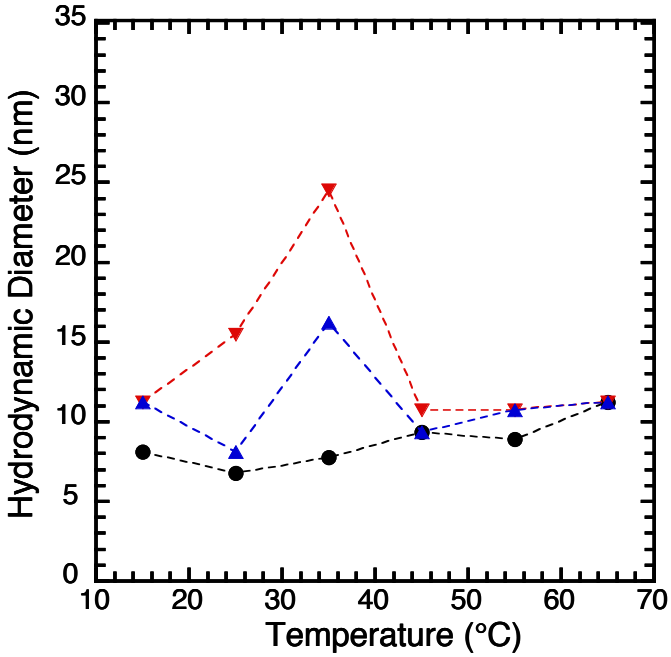

Figure A 1: Evolution of hydrodynamic diameter as function of temperature of (●) T15-S-30-DLS-0 ▼heating of T15-S-30-DLS-10, and ▲cooling of T15-S-30-DLS-10.

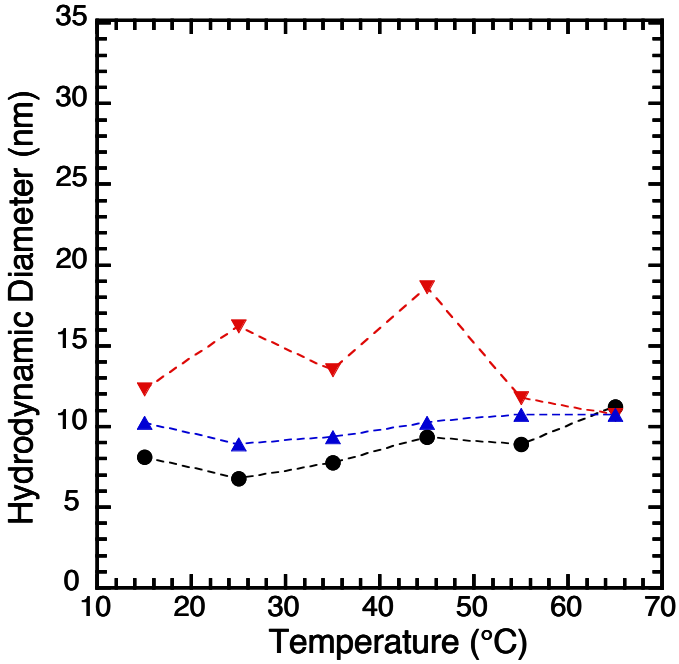

Figure A 2: Evolution of hydrodynamic diameter as function of temperature of (●) T15-S-30-DLS-0 ▼heating of T15-S-30-DLS-20, and ▲cooling of T15-S-30-DLS-20.

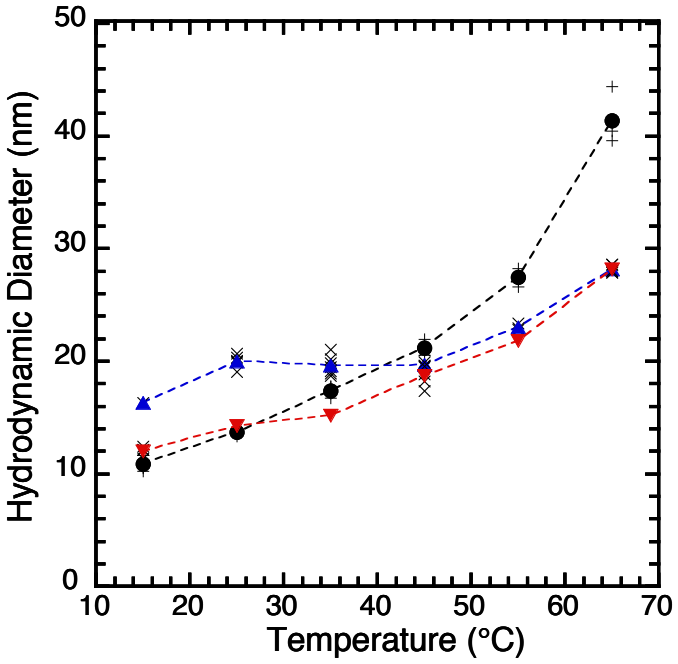

Figure A 3: Evolution of hydrodynamic diameter as function of temperature of (●) TNP-10-DLS-0 ▼heating of TNP-10-DLS-10, and ▲cooling of T15-S-30-DLS-10.

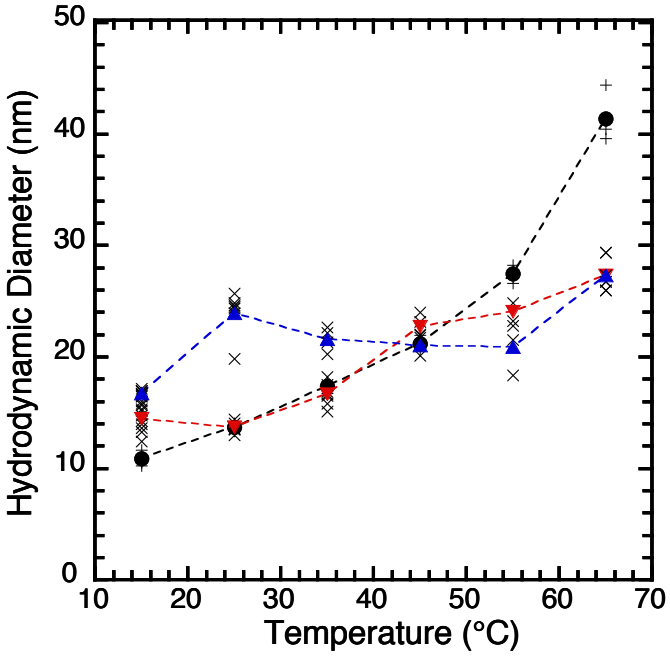

Figure A 4: Evolution of hydrodynamic diameter as function of temperature of (●) TNP-10-DLS-0 ▼heating of TNP-10-DLS-20, and ▲cooling of T15-S-30-DLS-20.

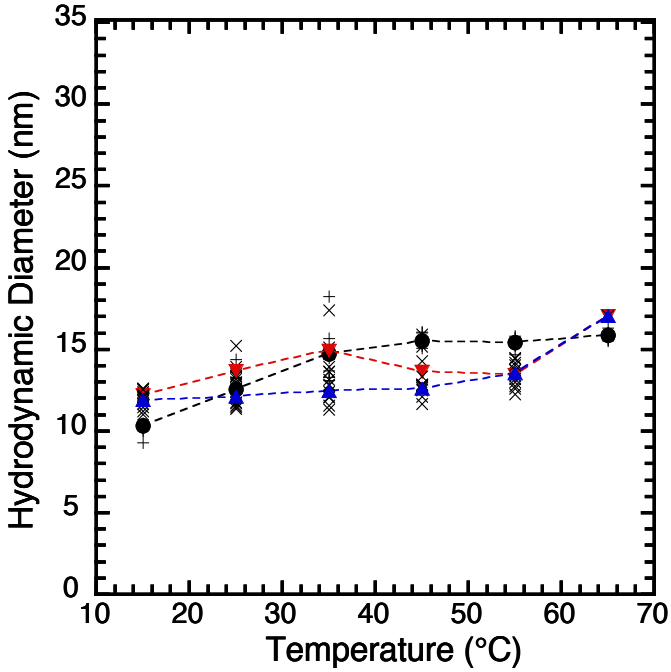

Figure A 5: Evolution of hydrodynamic diameter as function of temperature of (●) Tween20-DLS-0 ▼heating of Tween20-DLS-20, and ▲cooling of Tween20-DLS-20.

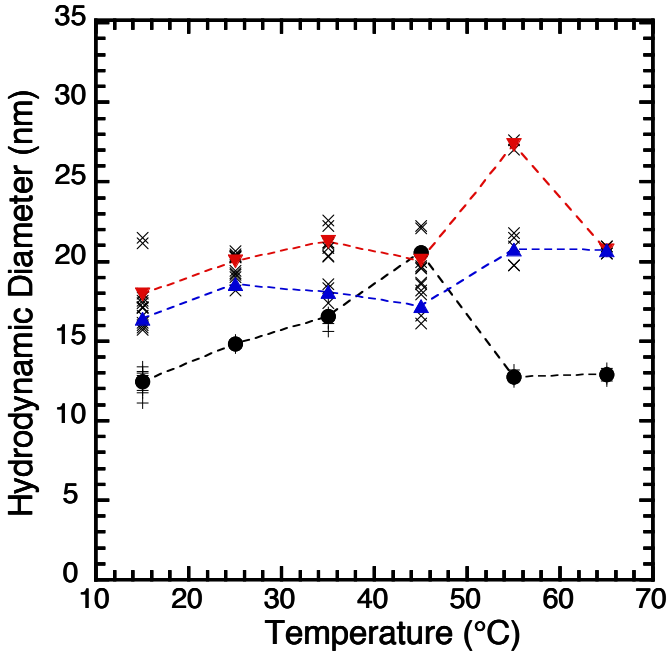

Figure A 6: Evolution of hydrodynamic diameter as function of temperature of (●) Brij98-DLS-0 ▼heating of Brij98-DLS-10, and ▲cooling of Brij98-DLS-10.

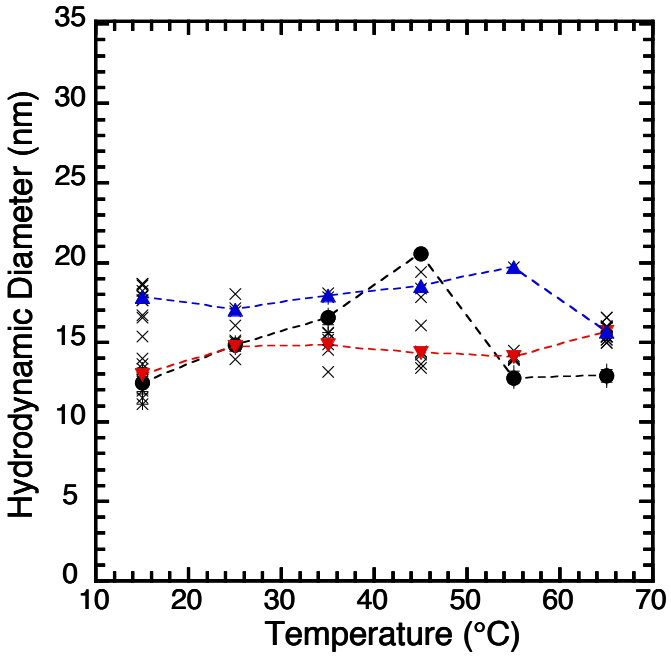

Figure A 7: Evolution of hydrodynamic diameter as function of temperature of (●) Brij98-DLS-0 ▼heating of Brij98-DLS-20, and ▲cooling of Brij98-DLS-20.

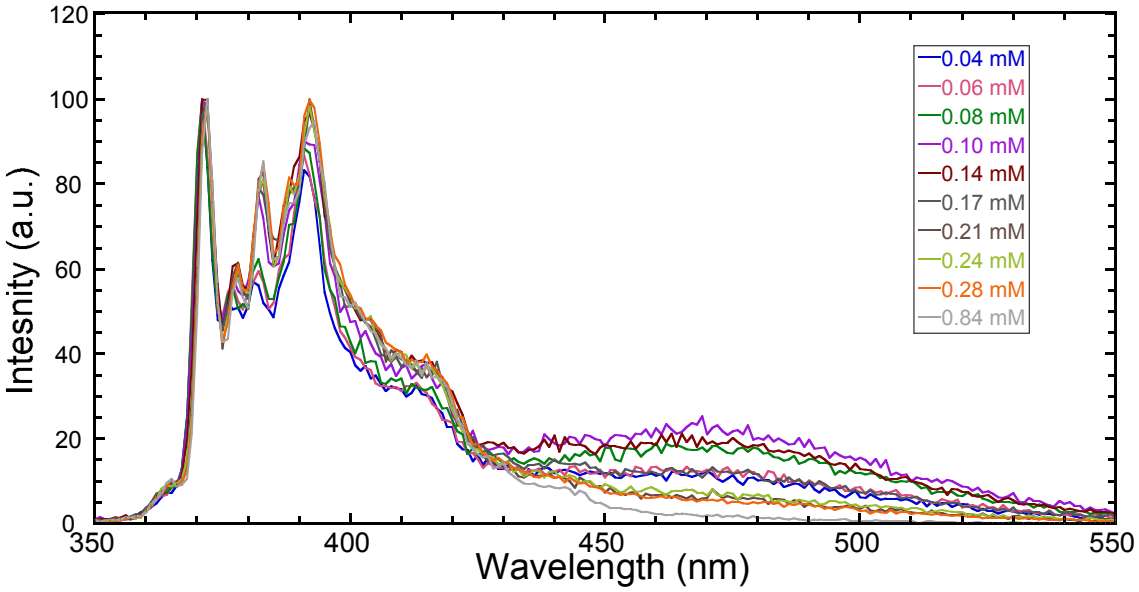

Figure A 8: Normalized steady state fluorescence spectra for T15-S-12/FSS/0/c series

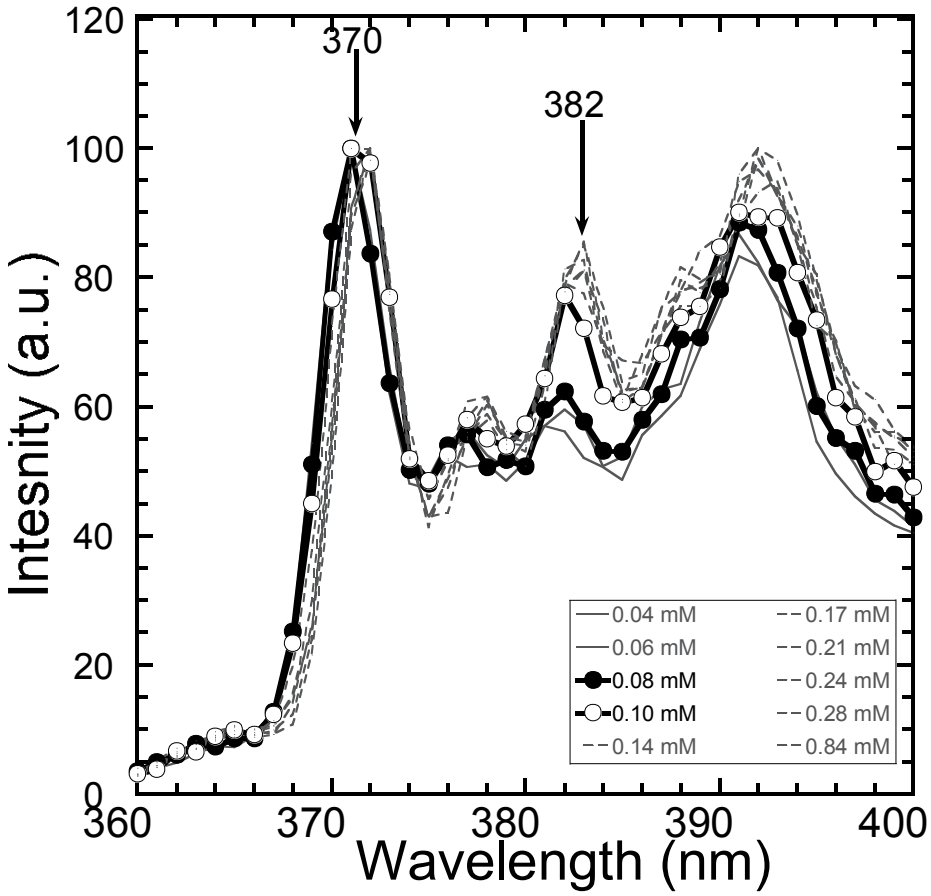

Figure A 9: Zoom in of normalized steady state fluorescence spectra for T15-S-12/FSS/0/c series showing the I1 (370 nm) and I3 (382 nm (peaks)

Table A 1: Relevant Parameters for Lifetime Fluorescence Analysis (Pure Micelle and TEOS:Surf 5)

Surfactant Only				*TEOS:Surfactant 5*			
[Py] (µM)	**<n>**	**k_q (s^{-1})**	**K_{exch}**	**[Py] (µM)**	**<n>**	**k_q (s^{-1})**	**K_{exch}**
1.91	0.3786	0.0102	187.1	0.793	0.1419	0.0095	192.7
9.56	1.5982	0.0114	177.9	0.798	0.2282	0.0086	230.8
7.33	1.1861	0.0111	185.6	3.22	0.5604	0.0096	189.9
2.06	0.4221	0.110	185.7	4.32	0.8535	0.0084	195.3
4.47	0.7987	0.0108	191.7	5.42	0.9438	0.0090	205.6
				8.08	1.4017	0.0092	212.6
				9.56	1.6873	0.0097	205.4

Table A 2: Relevant Parameters for Lifetime Fluorescence Analysis (TEOS:Surf 10 and 15)

TEOS:Surfactant 10				*TEOS:Surfactant 15*			
[Py] (µM)	**<n>**	**k_q (s^{-1})**	**K_{exch}**	**[Py] (µM)**	**<n>**	**k_q (s^{-1})**	**K_{exch}**
1.40	0.3181	0.0097	198.9	0.307	0.1924	0.0058	230.7
1.84	0.3586	0.0096	192.0	0.684	0.2366	0.0072	214.6
3.19	0.6472	0.0098	212.9	3.27	0.5816	0.0089	212.2
4.05	0.7591	0.0102	212.3	4.63	0.8933	0.0082	196.9
6.19	1.1744	0.0106	194.0	5.24	1.0569	0.0086	207.8
				7.97	1.4859	0.0093	227.0
				9.91	1.7385	0.0094	210.6

Appendix B: Silica HPLC Beads

Table B 1: Chemical Composition of HPLC_Brij98_y_T Series

Surfactant (g)	TEOS (g)	Water pH2 (mL)	NaF %	Alginate (g)	Temperature (^{0}C)	Surface Area (m^2/g)
4.92	18.2	60.6	8	1.165	25	137.9
4.92	18.2	60.6	16	1.165	25	6.0
4.92	18.2	60.6	24	1.165	25	6.1
4.92	18.2	60.6	32	1.165	25	DNP

Table B 2: Chemical Composition of HPLC_Brij58_y_T Series

Surfactant (g)	TEOS (g)	Water pH2 (mL)	NaF %	Alginate (g)	Temperature (^{0}C)	Surface Area (m^2/g)
4.91	18.2	60.6	8	1.165	25	19.1
4.91	18.2	60.6	16	1.165	25	4.7
4.91	18.2	60.6	24	1.165	25	DNP
4.91	18.2	60.6	32	1.165	25	10.2
4.91	18.2	60.6	8	1.165	25	671.2
4.91	18.2	60.6	16	1.165	25	487.7
4.91	18.2	60.6	24	1.165	25	426.2
4.91	18.2	60.6	32	1.165	25	393.9

*Highlighted samples indicate TEOS solutions that were stored in the fridge overnight before adding the NaF

**DNP means that the surface area measurements were not performed

Table B 3: Chemical Composition of HPLC_Brij98_y_T Series

Surfactant (g)	TEOS (g)	Water pH2 (mL)	NaF %	Alginate (g)	Temperature (^{0}C)	Surface Area (m^2/g)
4.21	15.625	45	2	0.525	25	DNP
4.21	15.625	45	4	0.525	25	DNP
4.21	15.625	45	6	0.525	25	DNP
4.21	15.625	45	8	0.525	25	DNP

**DNP means that the surface area measurements were not performed

Table B 4: Chemical Composition of HPLC_Brij58_y_T Series

Surfactant (g)	TEOS (g)	Water pH2 (mL)	NaF %	Alginate (g)	Temperature (^{0}C)	Surface Area (m^2/g)
4.21	15.625	45	2	0.525	25	DNP
4.21	15.625	45	4	0.525	25	DNP
4.21	15.625	45	6	0.525	25	DNP
4.21	15.625	45	8	0.525	25	DNP

**DNP means that the surface area measurements were not performed

Table B 5: Chemical Composition of HPLC_T15-S-12_y_T Series

Surfactant (g)	TEOS (g)	Water pH2 (mL)	NaF %	Alginate (g)	Temperature (^{0}C)	Surface Area (m^2/g)
2.775	15.625	45	2	0.5	20	70.5
2.775	15.625	45	4	0.5	20	7.9
2.775	15.625	45	6	0.5	20	6.7
2.775	15.625	45	8	0.5	20	6.4
2.775	15.625	45	2	0.5	25	8.2
2.775	15.625	45	4	0.5	25	6.9
2.775	15.625	45	6	0.5	25	7.1
2.775	15.625	45	8	0.5	25	6.5
2.775	15.625	45	2	0.5	30	DNP
2.775	15.625	45	4	0.5	30	DNP
2.775	15.625	45	6	0.5	30	DNP
2.775	15.625	45	8	0.5	30	DNP

**DNP means that the surface area measurements were not performed

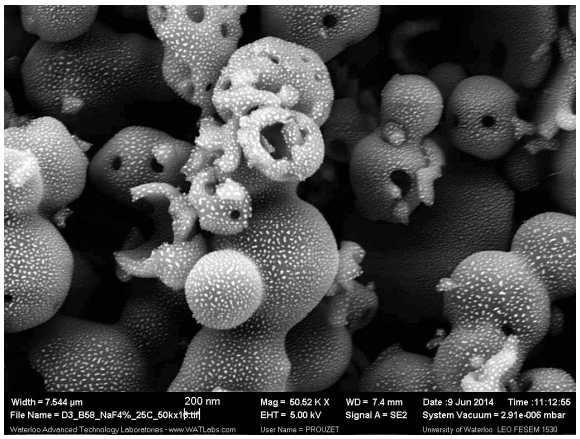

Figure B 1: SEM of HPLC_Brij58_4_25

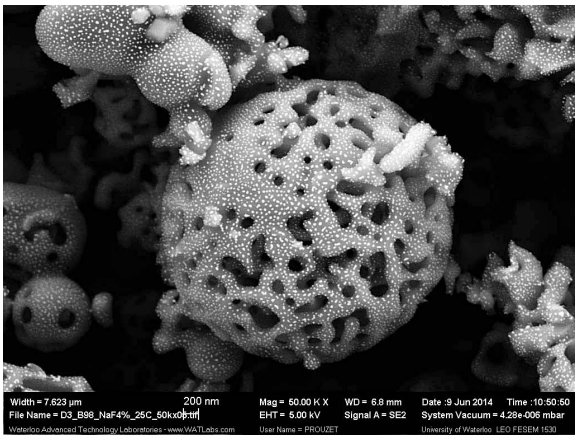

Figure B 2: SEM of HPLC_Brij98_4_25

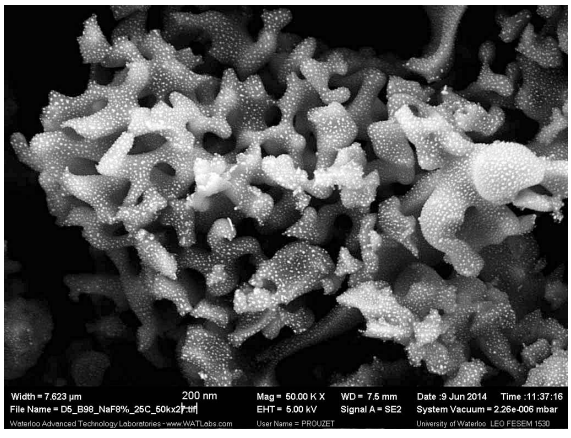

Figure B 3: SEM of HPLC_Brij98_8_25

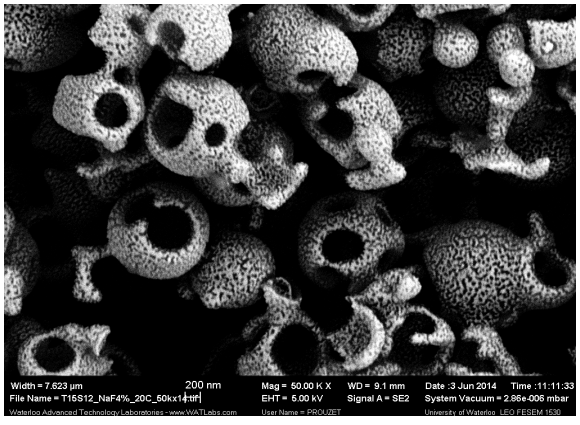

Figure B 4: SEM of HPLC_T15-S-12_4_20

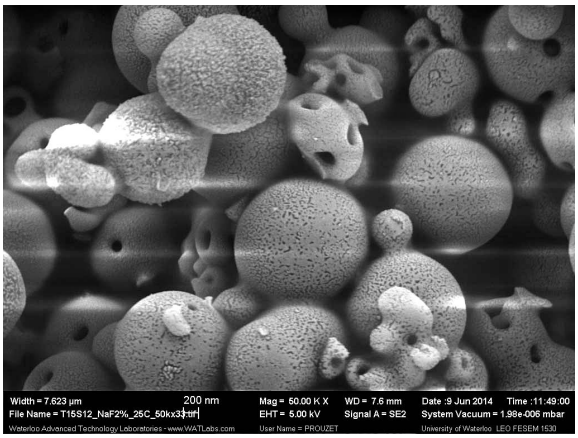

Figure B 5: SEM of HPLC_T15-S-12_2_25

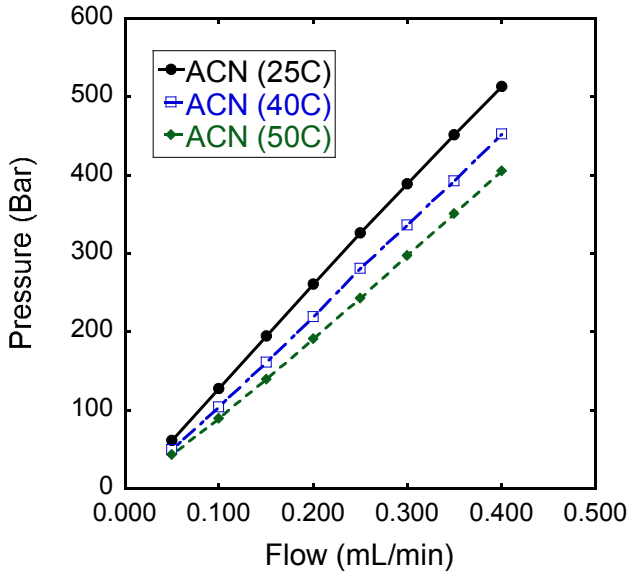

Figure B 6: Pressure as Function of Flow Rate of ACN in HPLC_T15-S-12_6_20 Packed Column

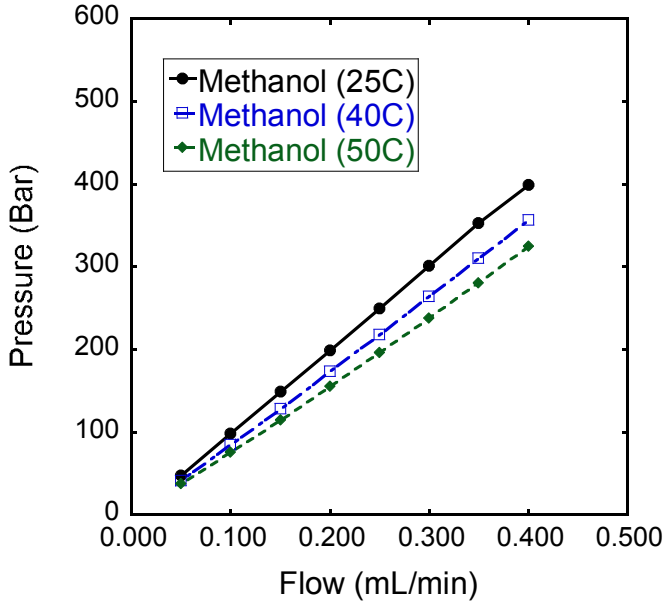

Figure B 7: Pressure as Function of Flow Rate of Methanol in HPLC_T15-S-12_6_20 Packed Column

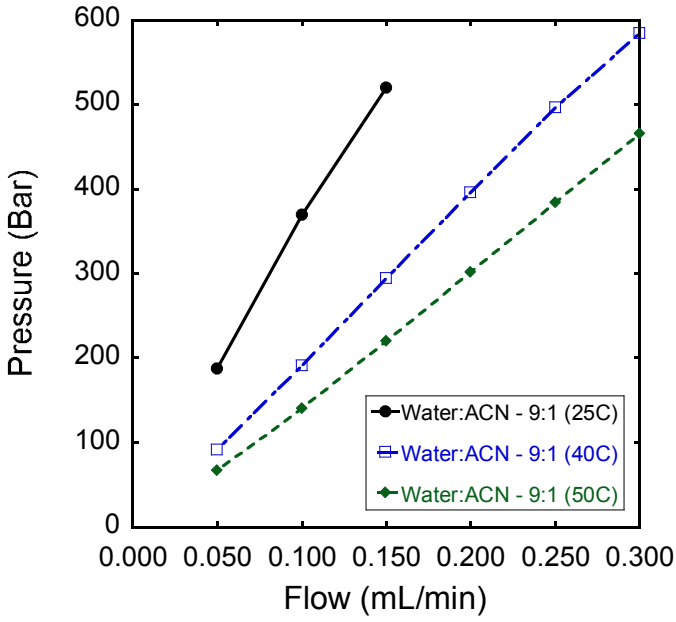

Figure B 8: Pressure as Function of Flow Rate of 9:1 Ratio of Water:ACN in HPLC_T15-S-12_6_20 Packed Column

Appendix C: Nanoemulsions and PBA-MSU

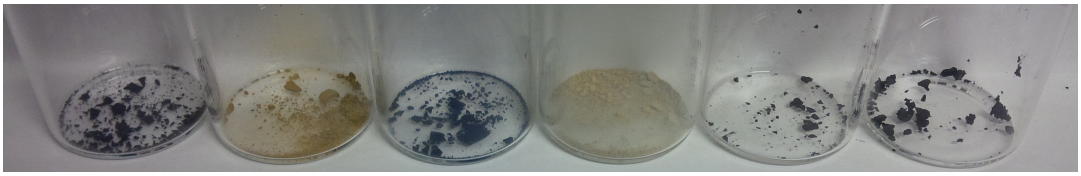

Figure C 1: (Left to Right): $Fe[Fe(CN)_6]$, $Ni_3[Fe(CN)_6]_2$, $Fe_3[Fe(CN)_6]_2$, $Sm[Fe(CN)_6]$, $Cu_3[Fe(CN)_6]_2$, $Co_3[Fe(CN)_6]_2$

Figure C 2: (Left to Right): $Fe_3[Co(CN)_6]_2$, $Co_3[Co(CN)_6]_2$, $Sm[Co(CN)_6]$, $Ni_3[Co(CN)_6]_2$, $Fe[Co(CN)_6]$, $Cu_3[Co(CN)_6]_2$

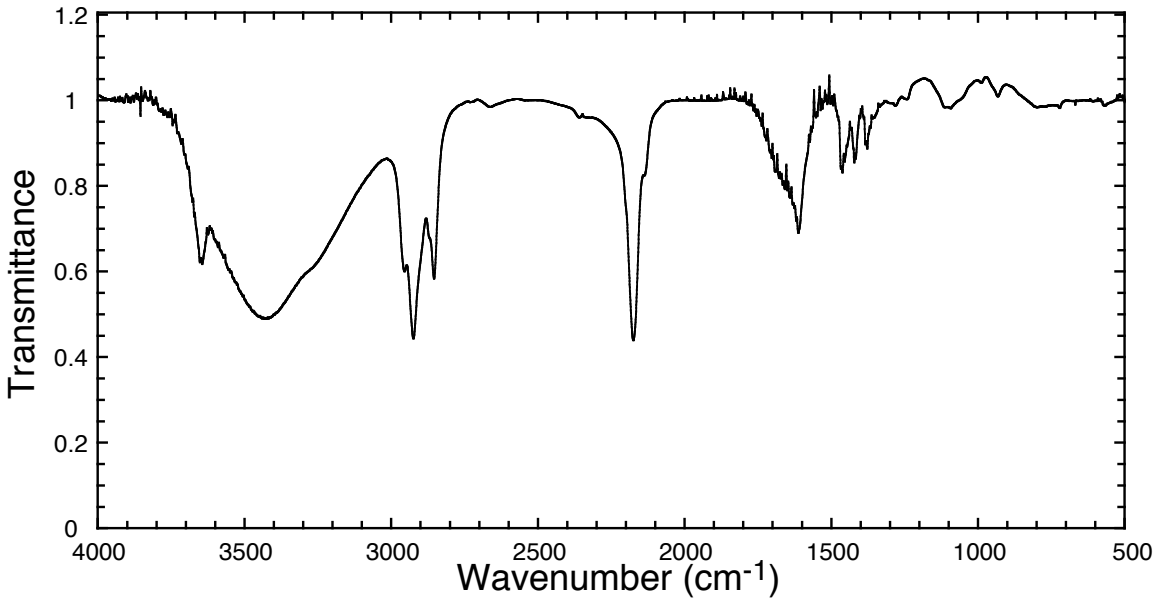

Figure C 3: FTIR Spectrum of $Co_3(Co(CN)_6)_2$ showing a distinct peak at approximately 2180 cm^{-1}

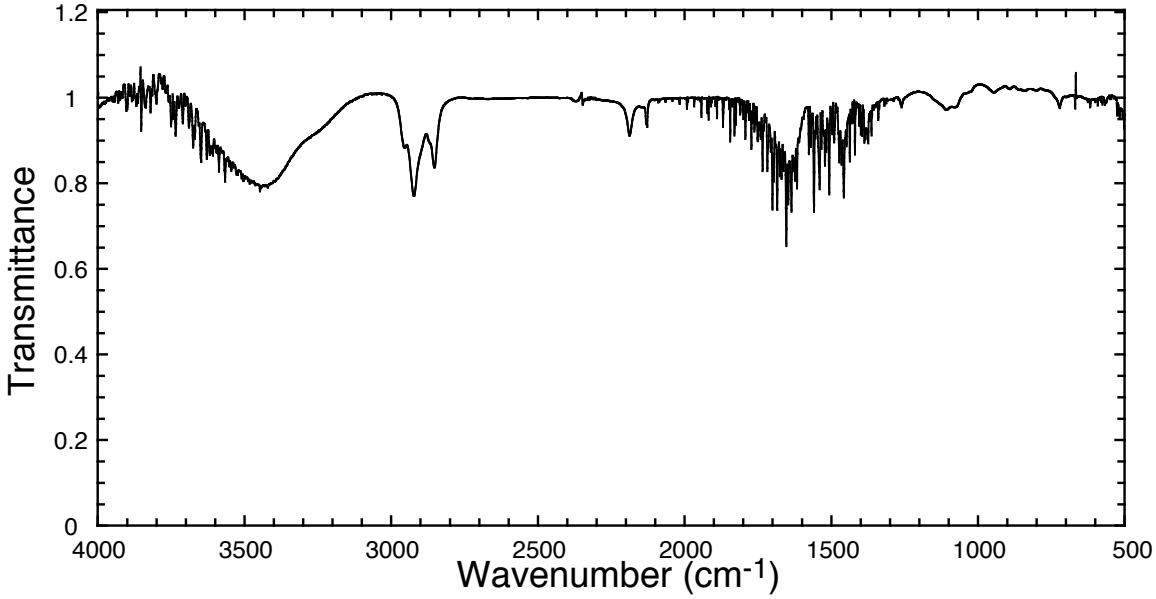

Figure C 4: FTIR Spectrum of $Cu_3(Co(CN)_6)_2$ showing a distinct peak at approximately 2180 cm^{-1}

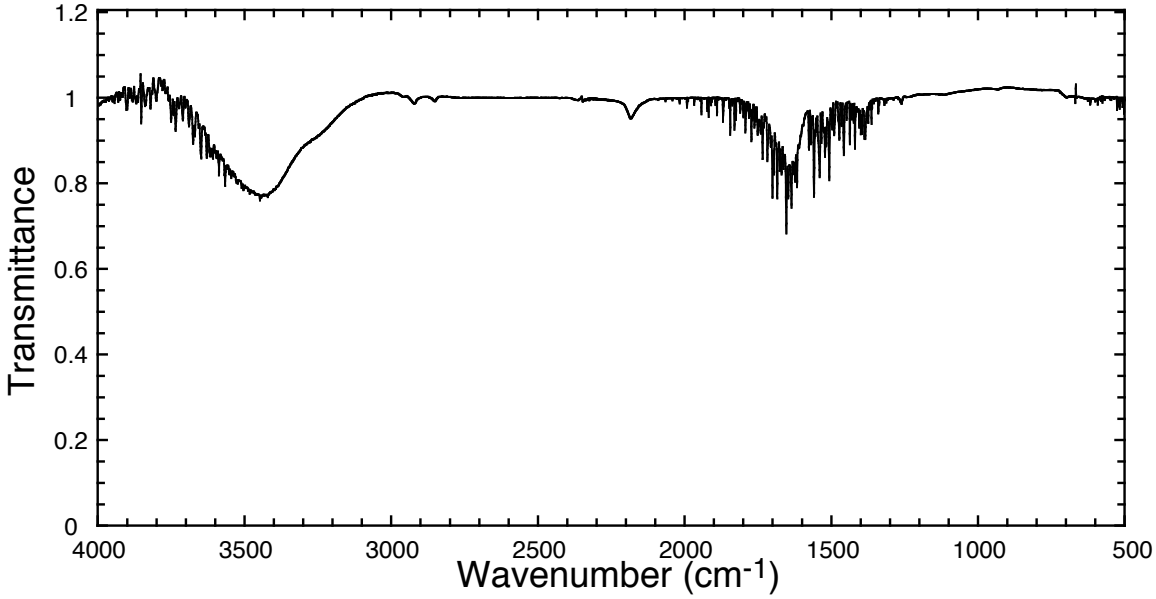

Figure C 5: FTIR Spectrum of $Fe(Co(CN)_6)$ showing a distinct peak at approximately 2180 cm^{-1}

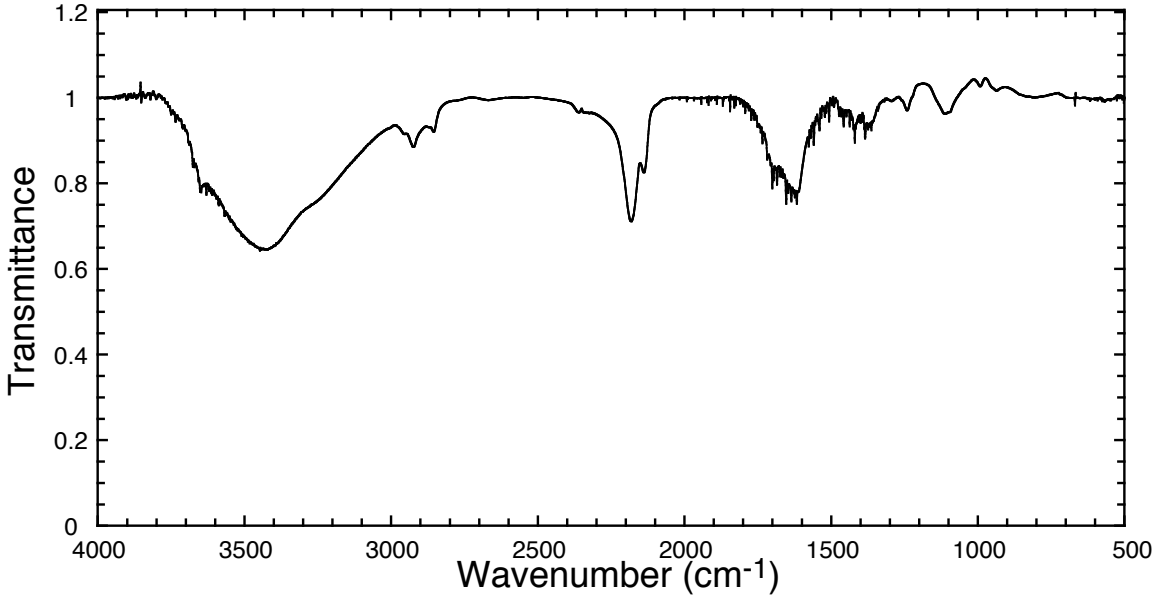

Figure C 6: FTIR Spectrum of $Ni_3(Co(CN)_6)_2$ showing a distinct peak at approximately 2180 cm^{-1}

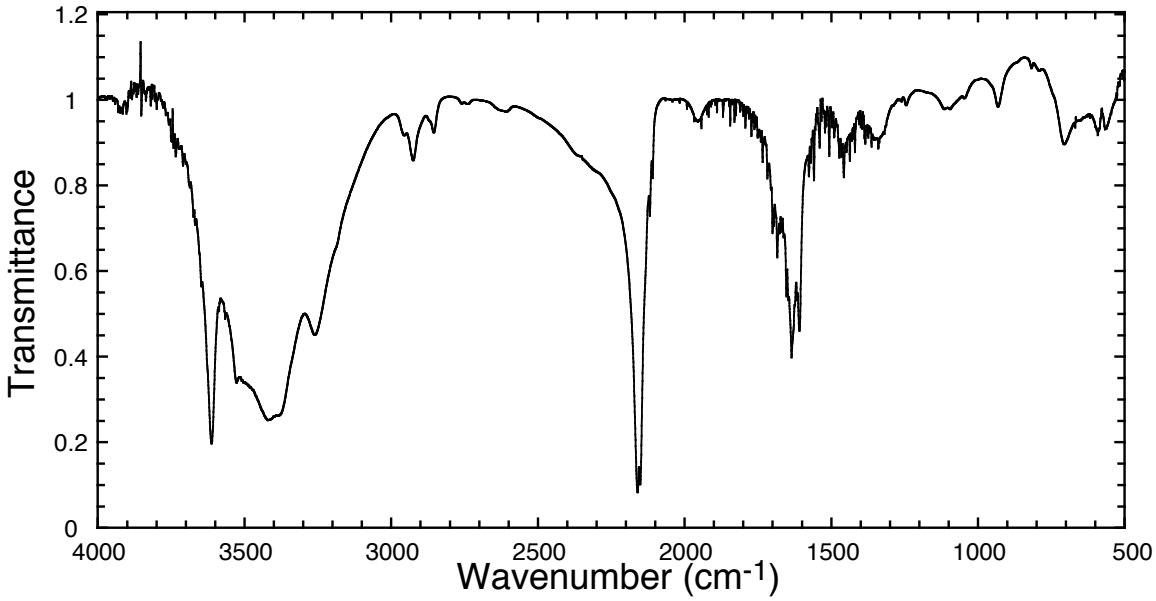

Figure C 7: FTIR Spectrum of $Sm(Co(CN)_6)$ showing a distinct peak at approximately 2180 cm^{-1}

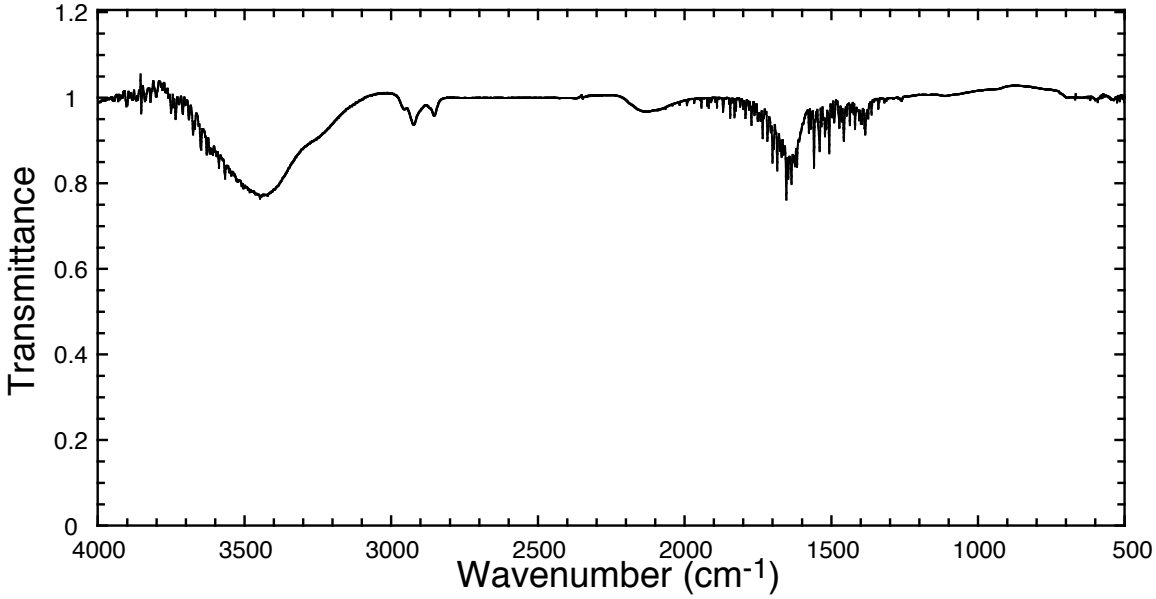

Figure C 8: FTIR Spectrum of $Co_3(Fe(CN)_6)_2$ showing a broad peak at approximately 2180 cm^{-1}

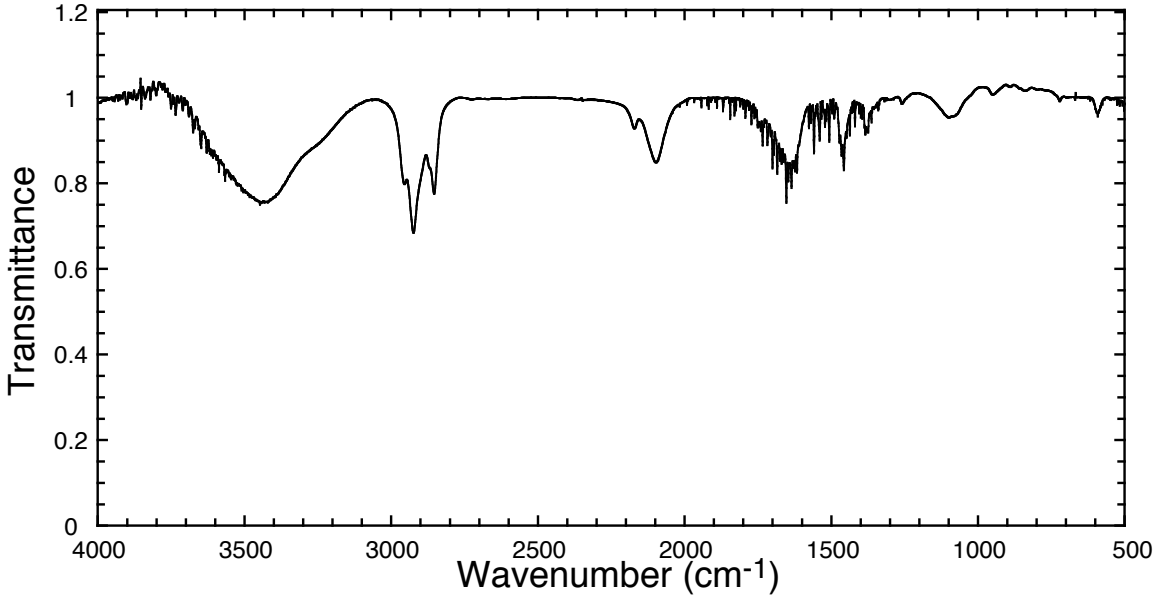

Figure C 9: FTIR Spectrum of $Cu_3(Fe(CN)_6)_2$ showing a distinct peak at approximately 2180 cm^{-1}

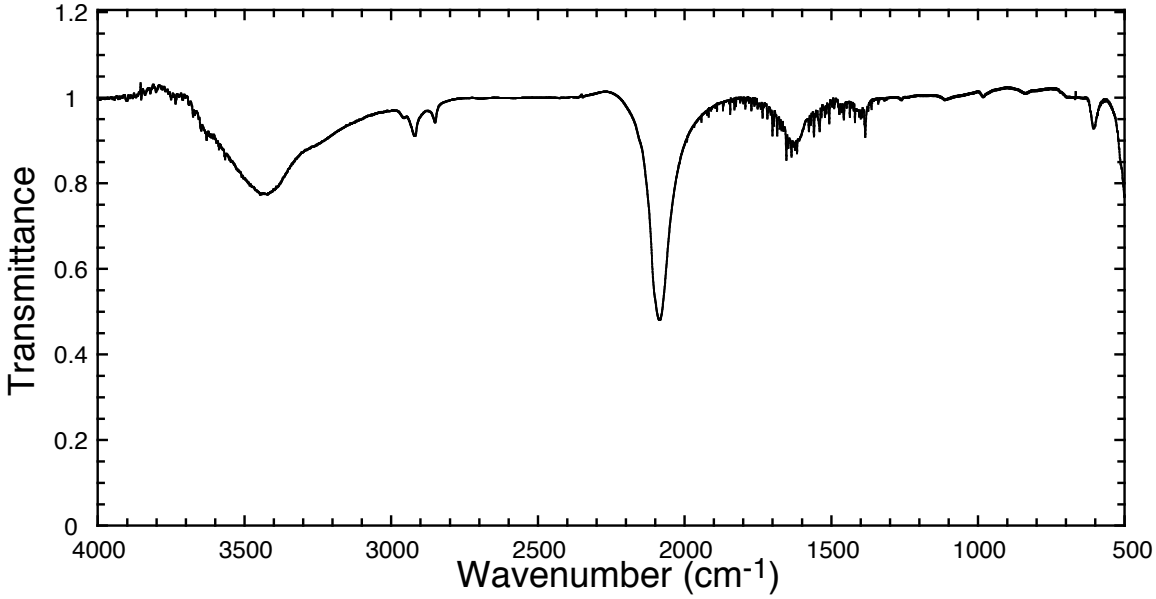

Figure C 10: FTIR Spectrum of $Fe(Fe(CN)_6)$ showing a distinct peak at approximately 2100 cm^{-1}

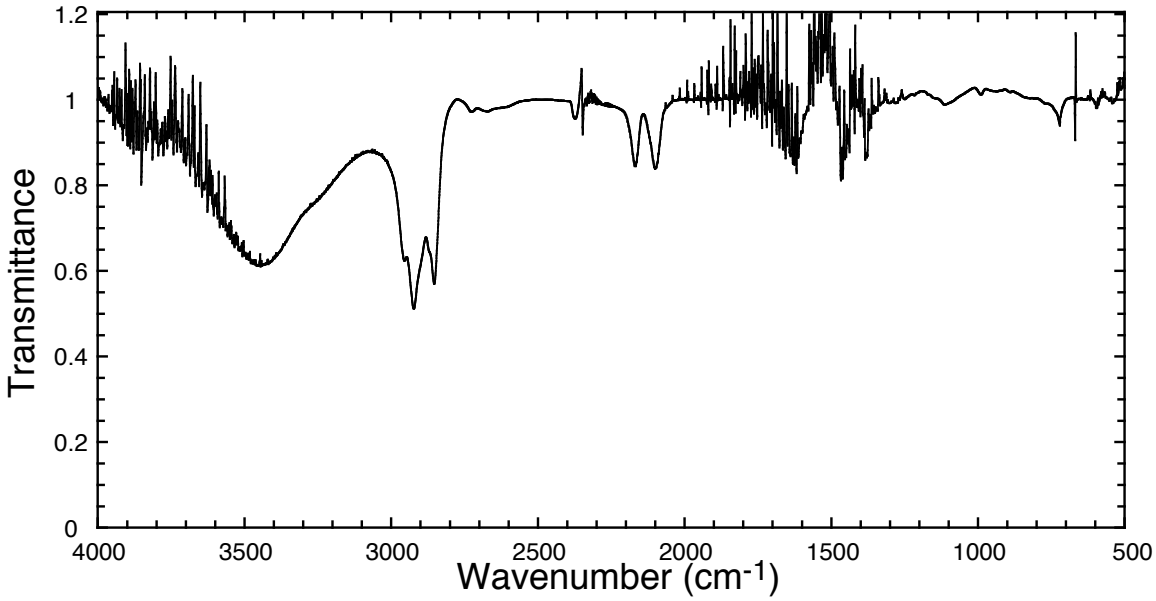

Figure C 11: FTIR Spectrum of $Ni_3(Fe(CN)_6)_2$ showing a distinct peak at approximately 2180 cm^{-1}

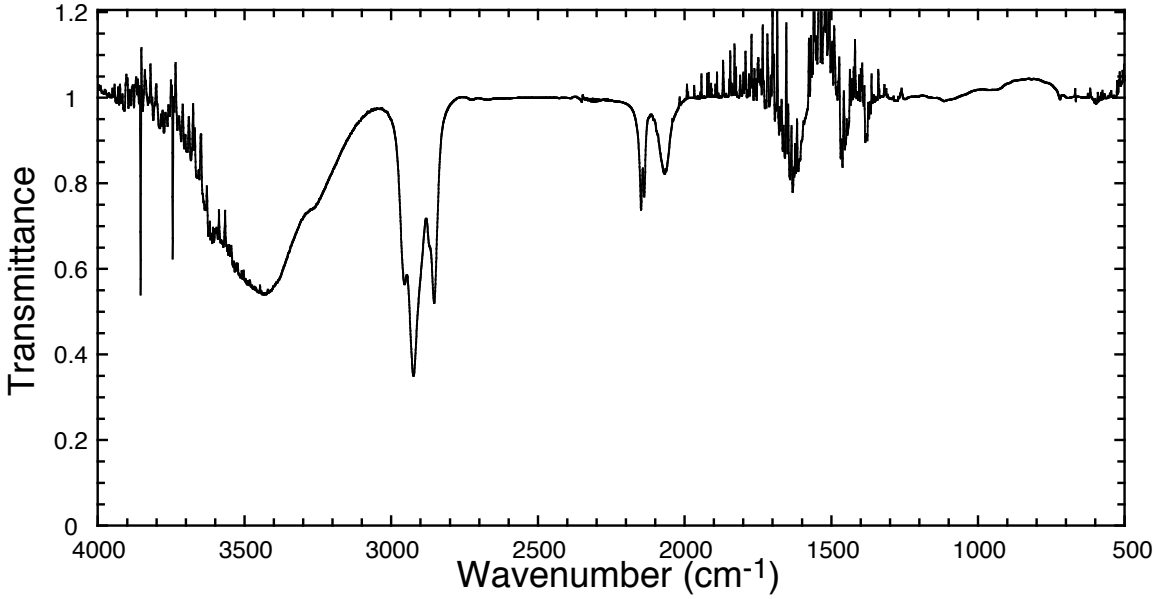

Figure C 12: FTIR Spectrum of $Sm(Fe(CN)_6)$ showing a distinct peak at approximately 2180 cm^{-1}

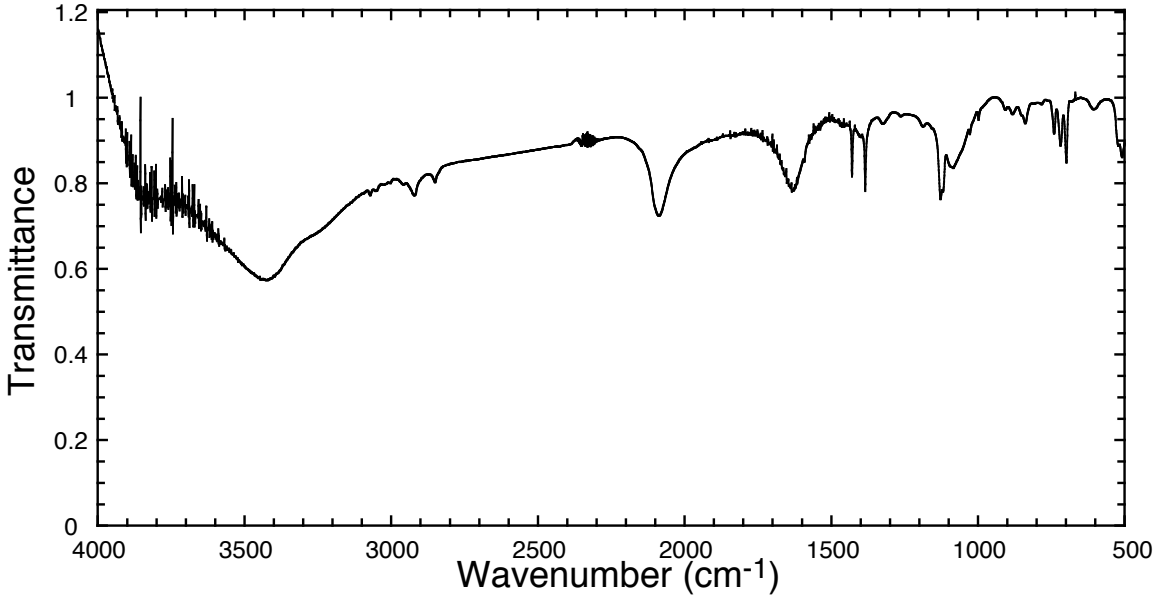

Figure C 13: FTIR Spectrum of $Fe_3(Fe(CN)_6)_2$ showing a distinct peak at approximately 2100 cm^{-1}

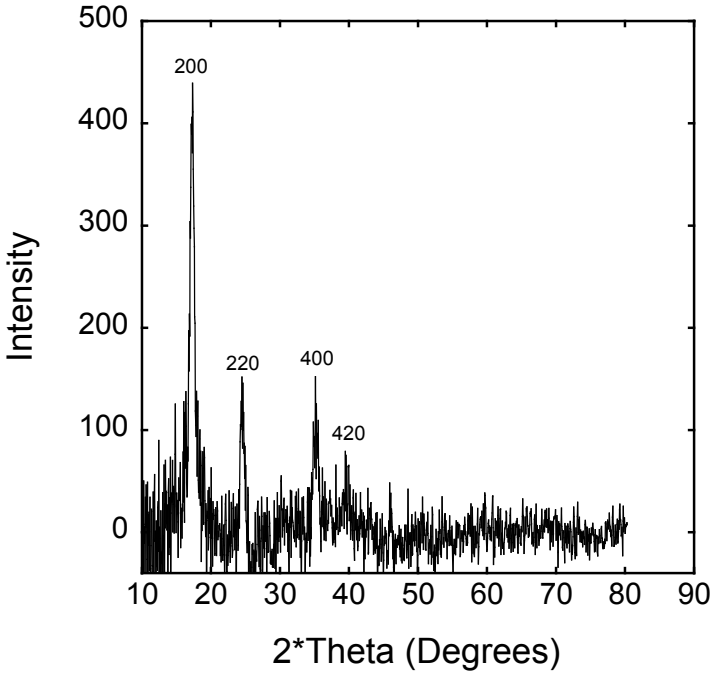

Figure C 14: XRD Pattern of $Ni_3(Co(CN)_6)_2$ showing clear diffraction peaks confirming Prussian Blue Analogue structure

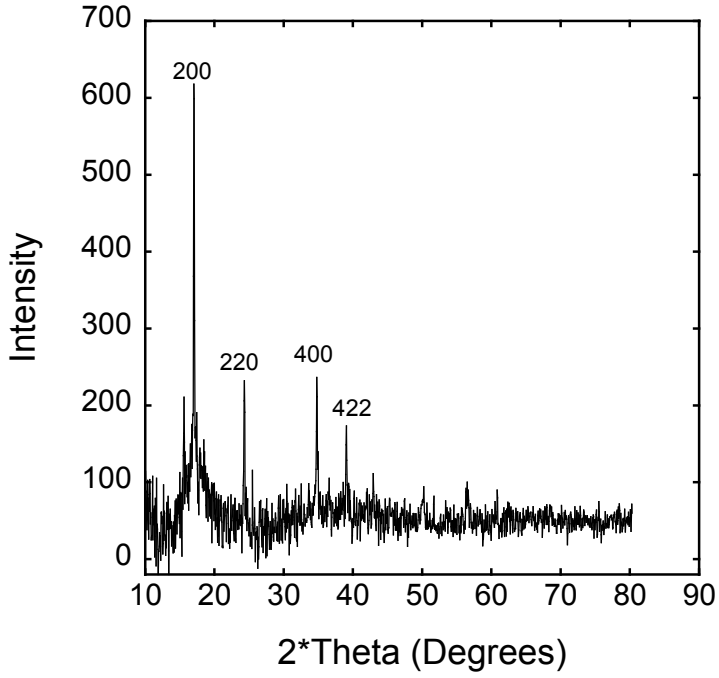

Figure C 15: XRD Pattern of $Co_3(Co(CN)_6)_2$ showing clear diffraction peaks confirming Prussian Blue Analogue structure